A Study on Self-Assembly of Organic Semiconductor Molecules on Vicinal Silicon Surfaces

微斜シリコン表面に於ける有機半導体分子の自己組織化の評価

A Dissertation Presented to
the Graduate School of Arts and Sciences
International Christian University
for the Degree of Doctor of Philosophy

国際基督教大学　大学院
アーツ・サイエンス研究科提出博士論文

January 30, 2021

SUZUKI, Yu
鈴　木　雄　宇

A Study on Self-Assembly of Organic Semiconductor Molecules on Vicinal Silicon Surfaces

微斜シリコン表面に於ける有機半導体分子の自己組織化の評価

A Dissertation Presented to
the Graduate School of Arts and Sciences
International Christian University
for the Degree of Doctor of Philosophy

国際基督教大学　大学院
アーツ・サイエンス研究科提出博士論文

January 30, 2021
２０２１年１月 30 日

SUZUKI, Yu
鈴　木　雄　宇

審査委員会メンバー

Members of Evaluation Committee

主査 / Chief Examiner

　岡野 健　　教授

副査 / Examiner

　田 旺帝　　教授

副査 / Examiner

　久保 謙哉 教授

副査 / Examiner

　髙桑 雄二　東北大学教授

Table of Contents

ABBREVIATIONS **3**

1 THE MOTIVATION OF THIS STUDY **1**

1.1 HOW TO FORM QUANTUM WIRE - ADVANCEMENT IN MICROELECTRONICS 1
1.2 ORGANIC MOLECULES WITH SELF-ASSEMBLY 2
1.3 MOLECULAR MOBILITY AND SUBSTRATE PASSIVATION: GOVERNING FACTORS FOR SELF-ASSEMBLY 6
1.4 SCOPE OF THIS STUDY 10

2 VICINAL SILICON SURFACE AND ORDERED STEP STRUCTURE **12**

2.1 THE MOTIVATION 12
2.2 EXPERIMENTALS 13
2.2.1 Ultra-High-Vacuum Scanning Tunneling Microscopy *13*
2.2.2 General surface topographical study and optimization *15*
2.3 RESULTS AND DISCUSSION 16
2.3.1 DC current flow direction dependence *16*
2.3.2 DC flash duration dependence *18*
2.3.3 DC flash energy dosage dependence *21*
2.3.4 Vicinal angle dependence on the vicinal silicon surface *26*
2.3.5 Surface reconstruction and the symmetry with vicinal surface *33*
2.4 SUMMARY 38

3 SELF-ASSEMBLY OF CUPC MOLECULES ON HYDROGEN PASSIVATED AND CLEAN VICINAL SILICON SURFACE **39**

3.1 THE MOTIVATION 39
3.2 EXPERIMENTAL 40
3.2.1 Si(111)-7x7 substrate preparation *40*
3.2.2 Hydrogen passivation on Si(111)-7x7 ..... *41*
3.2.3 CuPc deposition *42*
3.3 CUPC TOPOGRAPHY OBSERVATION WITH DOSE DEPENDENCE ON H-PASSIVATED SI SURFACE 43
3.4 THERMAL DESORPTION OF CUPC FROM HYDROGEN PASSIVATED SI(111)-7X7 50
3.5 CUPC DEPOSITION ON CLEAN SI(111)-7X7 SURFACE 51
3.6 SUMMARY 52

4 ANTIMONY PASSIVATED VICINAL SILICON SURFACE AND CUPC THIN FILM **54**

4.1 THE MOTIVATION 54
4.2 EXPERIMENTAL 56
4.2.1 Clean vicinal Si(111)-7x7 surface preparation *56*
4.2.2 Sb passivation *57*
4.2.3 CuPc deposition *58*
4.3 CUPC TOPOGRAPHY ON SB PASSIVATED STEPPED SI SURFACE 58
4.4 SUMMARY 72

5 ANALYSIS AND COMPARISON WITH THE RECENT STUDIES **73**

5.1 THE DIRECTION OF ONE-DIMENSIONAL GROWTH OF CUPC WITH RESPECT TO STEP EDGES 74

6 CONCLUSION **81**

7 ACKNOWLEDGMENT **84**

8 BIBLIOGRAPHY **85**

Abbreviations

Au	Gold
Ag	Silver
CuPc	Copper Phthalocyanine
DC	Direct Current
H	Hydrogen
LEED	Low Energy Electron Detraction
LT	Low Temperature
RMS	Root Mean Square
Sb	Antimony
Si	Silicon
STM	Scanning Tunneling Microscopy
UHV	Ultra High Vacuum

1 The motivation of this Study

1.1 How to form quantum wire - Advancement in microelectronics

The advancement of electronics has continuously had a substantial impact on the society and economy of modern life. Some of the examples of such advancement are, for instance, microprocessors with supreme calculation capacity, visual devices with devastatingly high spatial and color resolution. These are the achievements of modern technologies enabled by the tremendous amount of basic research on material science and electronics. The material sciences on semiconductor surfaces are of particular importance due to their wide variety of applications in modern electronic devices. [1, 2, 3, 4]

Solid-state physics formulated the understanding of the material characteristics such as electronic and optical properties by the periodic potential model in a superstructure. [5] The superstructure is a periodical construction of unit structures, *e.g.,* atoms, molecules. The material properties can be engineered by controlling the periodicity of atoms or molecules, forming a designated superstructure. The superstructure can be; three-dimensional when applied to the bulk properties, two-dimensional when applied to the interface between two materials, one-dimensional when applied to wires, or zero-dimensional for dots. Along with the further needs in the semiconductor industrial applications, a wide variety of materials is studied to identify promising candidates that can bring the designated superstructure into reality. [6, 7]

To form the superstructure, however, the techniques such as the photolithography or bottom-up approach, *e.g.,* single molecular manipulation [8, 9, 10], may possess challenges in achieving atomic level topographical order, engineering viability, or the speed of the manufacturing process to obtain a meaningful amount of the superstructure for realistic devices. [2, 3, 4]

1.2 Organic molecules with self-assembly

The self-assembly nature of organic molecules is a promising candidate for forming such superstructures in a fast and reliable fabrication process. Many types of organic molecules are already used in electronic device applications due to their variable nature in electronic and physical properties. [11, 12, 13, 14]

To fabricate a novel organic-inorganic hybrid device, it is essential to understand and control the organic molecules' self-assembly nature on the inorganic semiconductor surfaces. [15, 16, 17] One promising idea to induce the self-assembly of the organic molecules on the inorganic semiconductor surface is to utilize the nanoscale structure on the semiconductor surface. The self-assembly of organic molecules is a result of the affinity or repulsion of the unit molecular structure. A crystal of any molecule is one example of the self-assembly nature. The crystal structure is defined by the nature of the molecules how they aggregate, resulting in forming a superstructure.

One method is to utilize the scanning probe technique to control the location of molecules. A straightforward approach is to manipulate a single atom or molecule by the tip of a scanning probe. [8, 9, 10] Such techniques can locate the molecules at a designated location deterministically. However, the whole process takes significant effort to fabricate a large-scale structure when considered for future device application, which is not realistic. A promising idea is demonstrated by combining the self-assembly nature by modifying the affinity of the substrate by inducing a change in chemical condition by the tip of the scanning probe technique. By altering the surface affinity only on a location on the surface, a molecule can be anchored to a designated pattern on the substrate. [15] The speed and precision can be improved in manipulating the organic molecules on an inorganic substrate. However, still, utilizing the scanning probe technique to alter the surface affinity requires significant effort to fabricate a large structure which is not realistic for device application. Thus, the future device application requires a technique that does not involve a scanning probe technique to alter the surface affinity to anchor a molecule. Such novel technique shall have the capability to construct a designated low-dimensional structure of organic molecules, *i.e.,* one or two-dimensional structure.

The vicinal surface of crystalline silicon has been proposed as a promising candidate as a template for hosting such superstructures. [6, 18, 19, 20, 21] It is also essential to form such superstructures combined with the already proven semiconductor technologies. Integrating the molecular self-assembly technique to the existing semiconductor technology can benefit from the paramount applications of semiconductor devices.

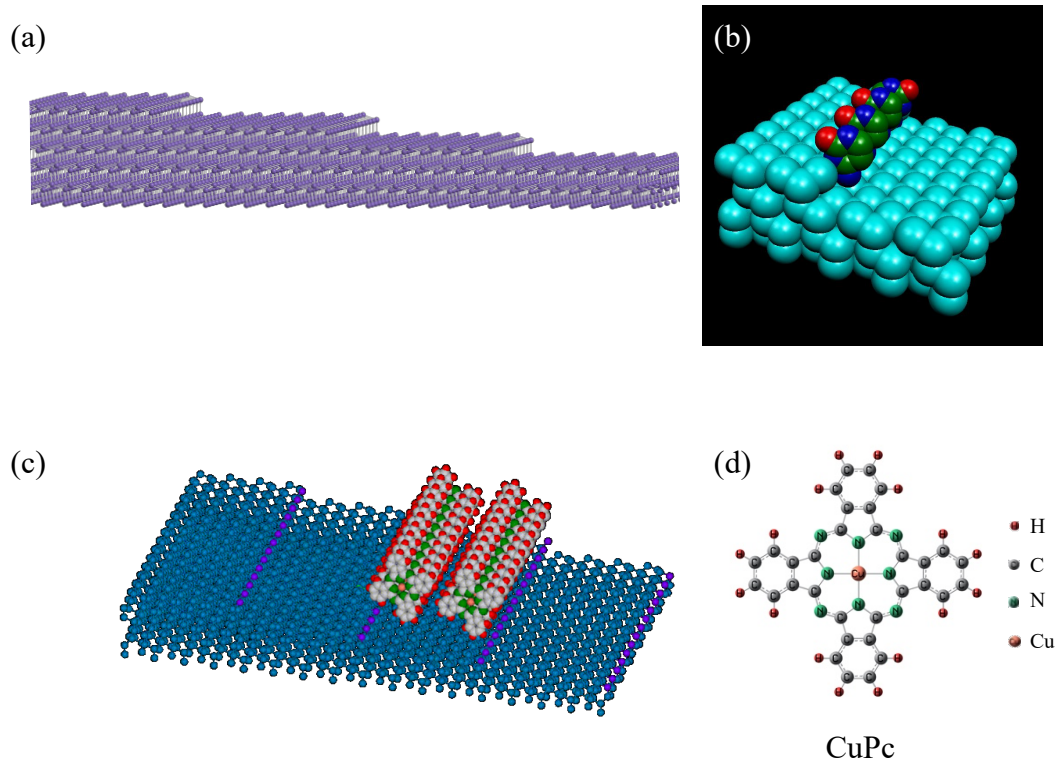

Fig. 1.1 (a) Image of vicinal silicon surface with atomic steps and terraces. (b) organic molecules, four Cytosine molecules, attached to a step edge. (c) Copper Phthalocyanine molecule forming one dimensional structure along the steps on atomically vicinal surface (d) CuPc single molecule

Vicinal silicon surface can serve as an ideal substrate to control the molecular superstructure formation on designated topographical locations while utilizing the existing semiconductor technologies. Vicinal surface, a subtle slope on a crystal silicon surface, having atomic layers steps may precipitate the formation of molecular superstructures. (Fig. 1.2) [18, 19, 20, 22] An insightful study was performed by Rauscher *et al.* to utilize the selective adsorption of organic molecules on a stepped structure on a vicinal silicon surface by controlling the surface affinity. [22] The study successfully demonstrates the potential of the vicinal silicon surface as a template for an organic molecule to form a low-dimensional structure. However, the alignment of single molecules into controlled self-assembly remained a challenge.

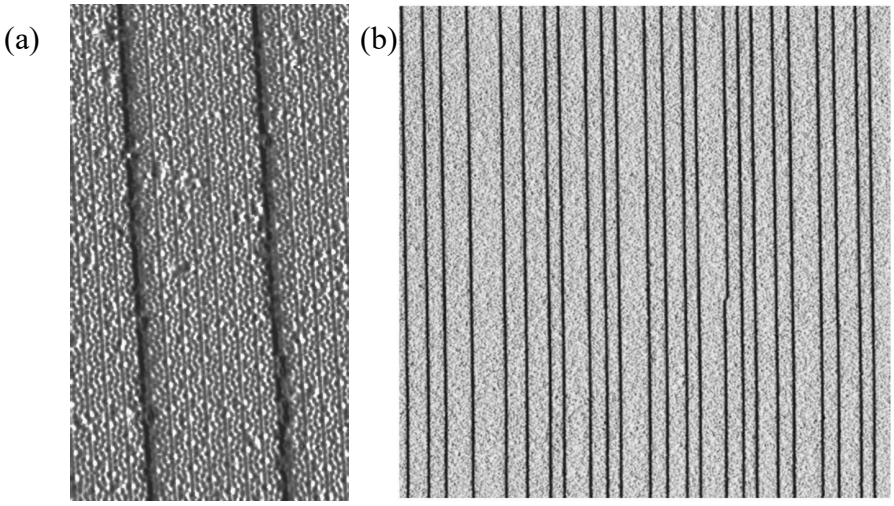

Fig. 1.2 Scanning tunneling microscopy image of two steps (dark lines) for a vicinal Si(111) 7x7 surface. (a) 40 x 70 nm^2 (b) 340 x 390 nm^2. Reproduced from *Lin et al.* [19], with the permission of AIP Publishing.

In order to induce such self-assembly, there are two essential conditions that the surface and the organic molecule need to meet. Firstly, there should be adequate molecular mobility on the surface to form a self-assembly structure. This is achieved by deactivating the dangling bonds on the surface by, for example, hydrogen. (Fig. 1.3) Secondly, at the same time, the anchoring the molecule at the designated location for fabricating the device structure, namely anchoring by the step edges. Namely, the dangling bonds on the terrace need to be deactivated, while those on the step edges are still active to anchor the organic molecules in order to induce the self-assembly utilizing the vicinal silicon surface.

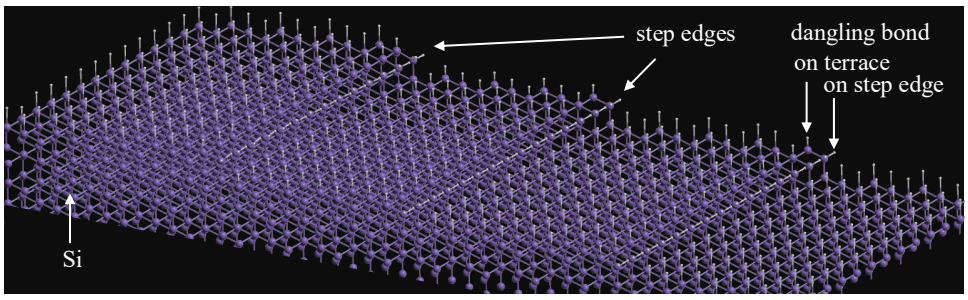

Fig. 1.3 A schematic model of a bare vicinal Si(111)1x1 surface. The surface dangling bonds are on the terraces and on the step edges as indicated by arrows on the right most step edge.

On the other hand, organic semiconductors are already utilized in device applications and widely studied in depths. [11, 12, 13] Amongst those materials, copper phthalocyanine (CuPc) is one of the materials which attracted attention from the early stage of organic semiconductor studies [1], and is shown to exert promising electric properties for device applications. [23, 24] There are extensive studies of CuPc on its electronic structure [25, 26, 27], as well as the crystallographic morphology on semiconductor surfaces. [28, 16, 29, 30]

Combining the vicinal silicon surface as a template to form an ordered organic semiconductor material structure has excellent potential as a building block for future novel device fabrication. This self-assembly method is expected to exert several advantages in order to fabricate the superstructure. Firstly, fast fabrication speed due to the intrinsic nature of the self-assembly process. The molecular self-assembly is faster compared to the single molecular manipulation by the mechanical probe technique. Secondly, the resulting superstructure is expected to exert molecular precision of the periodicity, which is expected from the crystallographic nature of the organic molecules.

1.3 Molecular mobility and substrate passivation: Governing factors for self-assembly

It is also essential to understand the effect of the interface between the organic molecules and the inorganic semiconductor surface, especially when the mechanical mo-

bility of the surface is largely affected by the binding energy of the molecule to the substrate. [31, 32, 33] To utilize the step structure of the vicinal silicon substrate, the ideal surface passivation is with the element that increases the mobility of the organic molecules while keeping the atomic structure of the vicinal silicon substrate.

Hydrogen passivation on a clean silicon surface is known to deactivate the surface and result in the self-assembly of organic molecules. [16, 28, 29] Hydrogen passivation is the straightforward choice to cap the dangling bonds on the vicinal silicon surface because atomic hydrogen is the minimum unit of an element. The purpose of this Study is to utilize the steps and terraces on the vicinal silicon surface. Thus, the surface passivation process is required to preserve the prepared vicinal silicon substrate's surface flatness. For this purpose, it is vital to seek minimal dimension and less complexity of the passivation element. Hydrogen is the first option from these perspectives.

However, hydrogen passivation on a silicon surface may show a variation of results depending on the experimental setup or passivation conditions, which may degrade the surface flatness, besides the challenges in experimental practicality. [34, 35, 36, 37, 38, 39]

The passivation by the atomic H leaves instability in the reproducibility of the quality of the surface conditions. One reason is the thermal effect on the sample surface by the filament during the atomic H passivation process. The irradiation of the filament may raise the temperature on the sample surface. The increased surface temperature is

reported to cause the deviation in the H passivation quality. [34, 35, 37, 36] Another reason is the possible chemical reaction of atomic H etches surface by forming silane, which may alter the surface's flatness, of which the degree of such effect deserves discussion. [38, 39, 36] In addition to these inherent challenges, the gaseous hydrogen requires controlled inlet with differential pumping technique to incorporate with the UHV-STM apparatus, which demands more effort in experimental procedures with reproducibility in a practical sense. When it comes to this method's potential industrialization, the entire surface preparation process should be assessed from the technique's practicality and accessibility to achieve the designated surface conditions.

The challenge with handling gaseous material, *i.e.,* H_2, can be solved by introducing solid material as a source of the passivation element. Amongst the available materials in the industrial practicality, the element shall cover only a single, if not several, monolayer on Si(111)-7x7 surface to preserve its step structure to achieve the objective of this Study. On the other hand, from the industrialization aspect, the monolayer-coverage process shall be stable and reproducible. Thus, it is ideal if the element can be deposited on the substrate for an arbitrary amount first. Then the excess element is desorbed, leaving only a single monolayer on Si(111) surface.

There can be several candidates for such elements, which may leave ordered thin atomic layers on Si(111)-7x7 substrate after thermal desorption. There are two criteria for choosing a suitable element. First is the chemical inertness when interfacing with organic molecules; in our case is CuPc. Second is the morphological behavior of the elements on

the Si(111)-7x7 surface after the thermal desorption process. Moreover, the thermal desorption process shall not exceed the critical temperature that induces the surface reconstruction on the Si(111)-7x7, in this case, is 850 °C, above which can induce the reconstruction to 1x1 and may alter the long-range order of step structure. [19, 21, 40]

From the chemical inertness, one example is Au and Ag on Si(111)-7x7. However, it is known to form aggregated islands when post annealed at elevated temperature rather than desorption of excess layers leaving the monolayer. [41, 42] Ni on Si(111) surface is known to form a uniform thin film by creating nickel silicide, preserving 7x7 reconstructed structure after annealing at 1000 °C. [43] Ga and In are reported to exert surface diffusion on Si(111), forming different surface reconstructions at different elevated temperatures. [44, 45, 46] However, when deposited for more than monolayer thickness, it is practically difficult to thermally desorb excess elements from the surface without altering the vicinal silicon substrate's step structure. For the element to desorb from the surface, the potential elements shall exert substantial vapor pressure under the process condition of this Study, *i.e.*, more than *ca.* 10^{-9} mbar, at a temperature lower than *ca*. 600 °C. [47, 48, 49]

Antimony (Sb), however, amongst other elements, is a suitable candidate for the objective of this Study. Antimony has been shown to cover the silicon surface with ordered atomic layers due to the stronger affinity between Sb-Si, than Sb-Sb interaction when deposited at certain surface temperature conditions. [50, 51, 52] Sb is a semimetallic

solid material, with a vapor pressure of 10^{-9} mbar at 520 °C, with the melting point at *ca.* 630 ºC under atmospheric pressure, which meets the conditions for the process of this Study. [47, 49] Sb is also chemically inert and can be handled without inducing a chemical reaction in ambient conditions. Sb is reported to preserve the Si(111)-7x7 reconstruction surface [53, 54], or Si(111)-1x1 reconstruction [54] after passivating the dangling bond on the silicon surface. Whichever the case, the interface between adsorbed Sb atoms forms uniform coverage on the Si substrate, preserving the atomic structure of the Si surface bilayer. This is also essential in selecting the surface passivation technique to utilize the atomically configured silicon vicinal surfaces.

1.4 Scope of this Study

In this Study, the potential of the vicinal silicon surface is demonstrated by utilizing its atomically ordered stepped surface as templates for ordering organic semiconductor molecules, CuPc. The Study investigates the effect of surface passivation elements, *i.e.,* hydrogen, antimony, or a clean silicon surface. The self-assembly behavior of CuPc on those surfaces is explored in-depth concerning the vicinal silicon surface's step structure. This Study expects to identify the potential effect of the step structure on the self-assembly nature of CuPc, with the molecular mobility induced by the surface passivation.

In Chapter 2, the vicinal silicon surface's topography and its preparation methods are studied in depths employing an ultra-high vacuum scanning tunneling microscope. The resulting vicinal silicon substrate will serve as the template substrate for the self-

assembly of organic molecules. In Chapter 3, the self-assembly nature of CuPc on hydrogen (H) passivated vicinal silicon substrate is studied. Self-assembly of CuPc with respect to the step edges of the vicinal silicon surface is shown. In Chapter 4, the self-assembly nature of CuPc on antimony (Sb) passivated vicinal silicon substrate is examined. On both H and Sb passivated vicinal silicon surface, CuPc exerted a highly oriented self-assembly nature, however, with a significant difference in the direction of CuPc orientation with respect to the surface and the steps on the vicinal silicon substrate. The results are discussed in Chapter 5, followed by the conclusion in Chapter 6.

2 Vicinal silicon surface and ordered step structure

2.1 The motivation

Controlling the topography of a semiconductor surface has considerable implications for various applications, not only from the scientific interest but also from industrial applications. Amongst such surface control, atomic precision is required for the ultimate technology for future material science and novel device fabrications.

The vicinal surface of crystalline material can be a candidate for such approaches to fabricate the atomically controlled surface structure. [19, 15] Due to the crystalline surface's nature, the atomic steps will be self-constructed with the multiples of atomic steps when the surface has a slight miscut angle; the vicinal surface. However, fabricating such crystal surfaces for device application requires further experimental studies to show the reproducibility of such techniques based on similar surface preparations. [55]

Amongst all the inorganic crystal materials, the monocrystalline silicon surface was chosen for this Study. This is because of the future implication of the organic-inorganic hybrid device application to make most of the conventional semiconductor process techniques. [6]

In this chapter, the vicinal silicon surface preparation is observed employing a scanning tunneling microscope under an ultra-high vacuum (UHV-STM). The surface topography is discussed for different vicinal angles and several parameters of surface preparation procedures to obtain atomically controlled stepped surface, as a precursor to the subsequent study with organic molecules on these surfaces.

2.2 Experimentals

2.2.1 Ultra-High-Vacuum Scanning Tunneling Microscopy

(111) oriented silicon wafer material with natural oxide on top was supplied by Silchem GmbH, Germany. Two different nominal miscut angles were prepared, namely 3° and 0.35°, with respect to $[111]$ surface normal. The miscut angle is tilted towards $[1\bar{1}0]$ direction. The step edges are thus parallel to $[\bar{1}01]$ direction, and the wafer's primary flat. The miscut angle of 0.35° was chosen as the result of the optimization procedure of the miscut angle dependency.

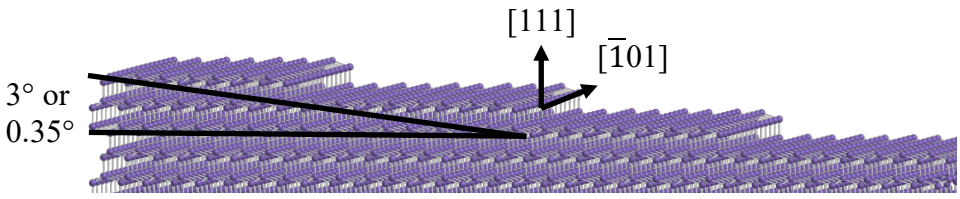

Fig. 2.1 Schematic of the vicinal silicon surface with its crystallographic orientation employed in this study

The wafer was cut into strips with a dimension of 1.0 x 15 mm^2. The cut silicon strips were then mounted on the sample holder capable of direct current heating, *i.e.,* current passes through the silicon strip. The silicon can be directly heated up to high temperatures. (Fig. 2.2) By alternating the silicon strip's mount direction, the current flow direction can be controlled with respect to the step edges on the silicon surface.

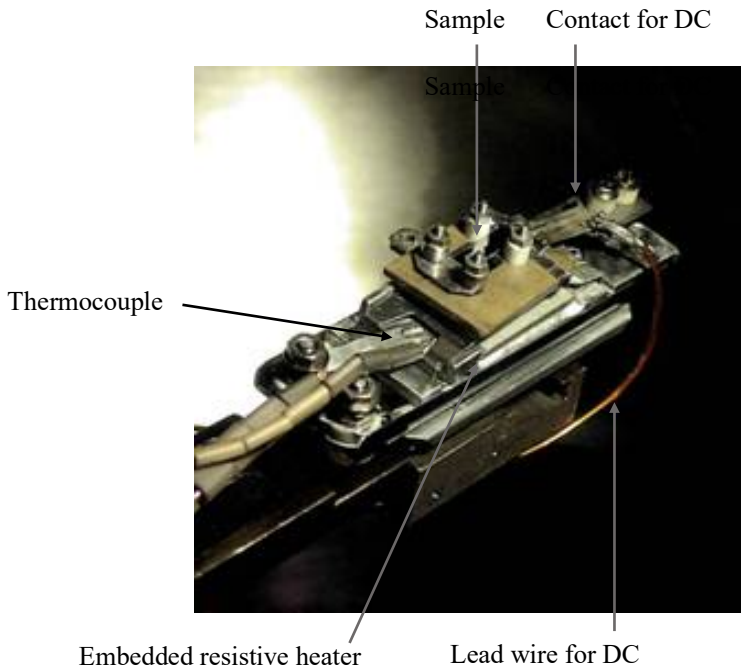

Fig. 2.2 UHV-STM Sample holder with direct-current heating fixture attachment

After mounting on the sample holder, the samples were transferred into an ultra-high vacuum scanning tunneling microscope (UHV-STM, Omicron GmbH, Germany, Fig. 2.3) chamber where the base pressure is lower than 2×10^{-10} mbar. Electrochemically etched tungsten was used for the STM tip. Under the UHV condition, the samples were degassed by a conventional ceramic heater at 700 °C for over 12 h until the base pressure was recovered.

Direct current (DC) heating is then performed in order to desorb the natural oxide layer and form atomically ordered steps and terraces on the vicinal surface. In general, the silicon strip was heated up to 750 °C, then flashed up to 1300 °C and kept for a certain

period. The detailed heating cycle parameters are optimized and described in the following section. The temperature of the sample at high temperature was monitored by an optical pyrometer (VF-3000, Optex Co., Ltd., Japan) throughout the experimental procedure to ensure the temperature and the DC flash duration.

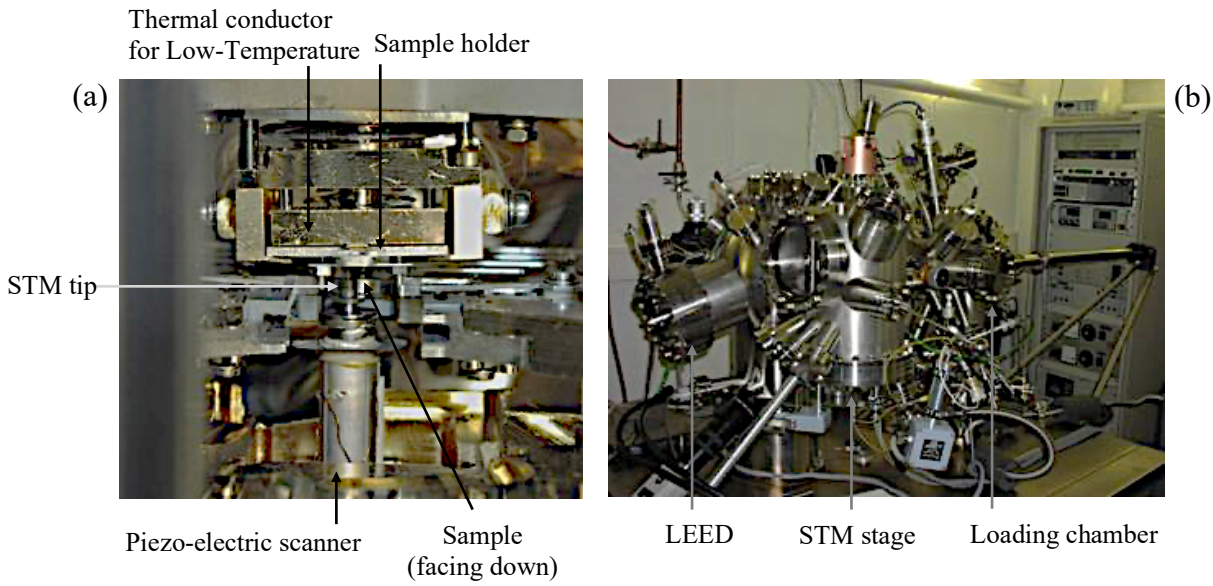

Fig. 2.3 (a) UHV-STM setup (b) Sample holder in the observation configuration

2.2.2 General surface topographical study and optimization

The detailed studies on the preparation procedure of the vicinal silicon surfaces were presented in the precedent reports. [6, 55, 56] From these studies, the effect of electromigration is expected on these vicinal surfaces at an atomic scale. [57] To utilize the effect of the electromigration for fabricating atomically straight step edges and flat terraces, two different DC current flow directions with respect to the vicinal surface were performed to compare the effect on the step edge morphologies. As depicted in the Experimentals of the previous section, the nominal vicinal angle was set to be perpendicular to the primary flat. In order to show the dependency of the current flow direction, the

current flow was either parallel (A), or perpendicular to the primary flat (B), as depicted in Fig. 2.4.

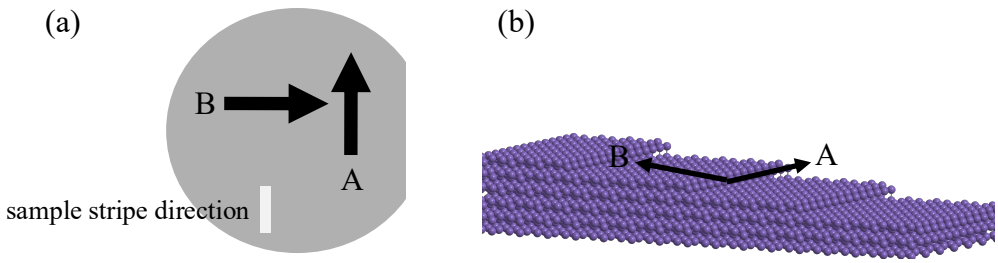

Fig. 2.4 Si(111) wafer crystal orientation and the DC flash current flow in this study. Either perpendicular (A) or parallel (B) current was applied. (a) The current direction and with respect to the primary flat of the wafer under study. The white cutout depicts the sample stripe direction with respect to the wafer orientation. (b) The current direction with respected to the step direction of the same wafer.

2.3 Results and discussion

2.3.1 DC current flow direction dependence

Fig. 2.5 shows the UVH-STM images of the silicon surface with the vicinal angle of 3°, (A) with the DC flown parallel and (B) perpendicular to the step edges, respectively. The DC current is applied to keep the sample temperature at 750 °C for 10 min and then flashed at 1300 °C for 3 min. These represent the general trend of the sample surface topography from multiple attempts of sample preparation. From these comparisons, there can be two main observation results are drawn. Firstly, the step edge morphology is drastically altered by the DC flow direction. Secondly, there are significant contaminants still left on the surface, which appear as white spots on the tips of the step edges.

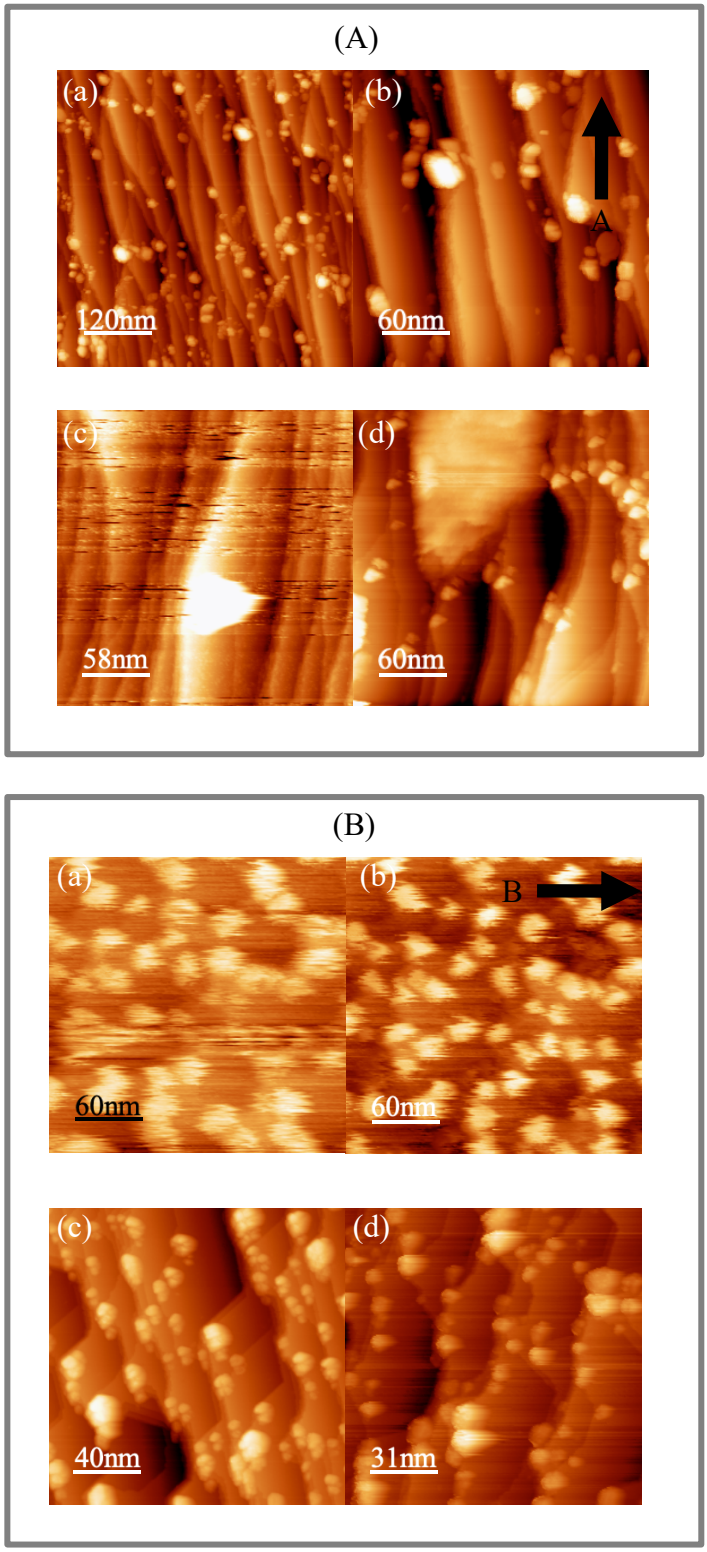

Fig. 2.5 (A) UHV-STM topographies of vicinal silicon surface with the DC current flown parallel to the step edges. 4 images represent typical sample surface measure from separate sample locations. Scanning area (a) 600 x 600 nm^2 (b) 300 x 300 nm^2 (c) 290 x 290 nm^2 (d) 300 x 300 nm^2, (B) DC flow perpendicular to the step edges. Scanning area (a) 300 x 300 nm^2 (b) 300 x 300 nm^2 (c) 200 x 200 nm^2 (d) 155 x 155 nm^2 (constant current mode, 1.7 nA, 2.3 V)

To the first point on the morphology of the step edges and the terraces, it can be generally claimed that the DC flow direction has a substantial influence on the step edge morphology. As expected, DC current flow dependence is promising when applied to the control of the step edges, as presumed in the thesis of this Study. At the same time, it also implies that since the morphology is significantly altered by the current flow, there must be an optimal condition for such DC flow dosage.

To the second point of the surface contaminants, it is difficult to conclude the contaminants' origin only from the UHV-STM topographical technique. The bright spots appearing under the UHV-STM image with the Constant-Current mode show the convolution of the conductance and the height of the surface structure. However, these contaminants are only speculated to be some leftover of the natural oxide layer on the silicon surface. If that is the case, it can be desorbed off by a higher dosage of the DC flash.

From the above observations, the DC flash current flow parallel to the step edges contributes to straighter step edges, reproducing the suggested electromigration effect reported in another study. [55]

2.3.2 DC flash duration dependence

In order to perform the DC flash dependence, the same silicon strips were cut out of the identical silicon wafer, namely a vicinal angle of 3°. In this comparison study, the

DC current was flown parallel to the step edges on all of the samples expecting the electromigration effect to straighten the step edges. The DC flash was performed only one time for each sample, with varying the duration of the flash. In order to remove the effect of the oxide layer thickness, the samples were prepared afresh for each flash dependency observation.

Fig. 2.6 shows the Constant-Current UHV-STM topographies on the samples after different DC flash durations, 20 sec, 30 sec, 180 sec, and 1.5 h for (a), (b), (c), (d), respectively. The samples' surface morphologies after 20 sec, 30 sec, and 180 sec of DC flashes exert similar step and terrace morphologies. Namely, there was no significant difference in the quality of the step edge morphology observed in these three DC flash durations. However, after 1.5 h of the DC process, the surface quality is significantly degraded, and difficult to observe the meaningful characteristic of the step edges. DC procedure for 1.5 h showed substantial degradation in Fig. 2.6 (d) compared to other samples with shorter flash durations. The blurred low contract image indicates the low conductivity on the surface, which can be attributed to surface contaminants.

Though the UVH-STM chamber has been kept under 1×10^{-9} mbar throughout the measurement, a substantially longer duration of the DC procedure may have resulted in the degassing from the sample mounting fixture. In fact, the pressure on the UHV-STM chamber was observed to have slightly increased though always kept under 1×10^{-9} mbar. This may explain the surface quality degradation due to the contaminants originating from the surrounding fixtures.

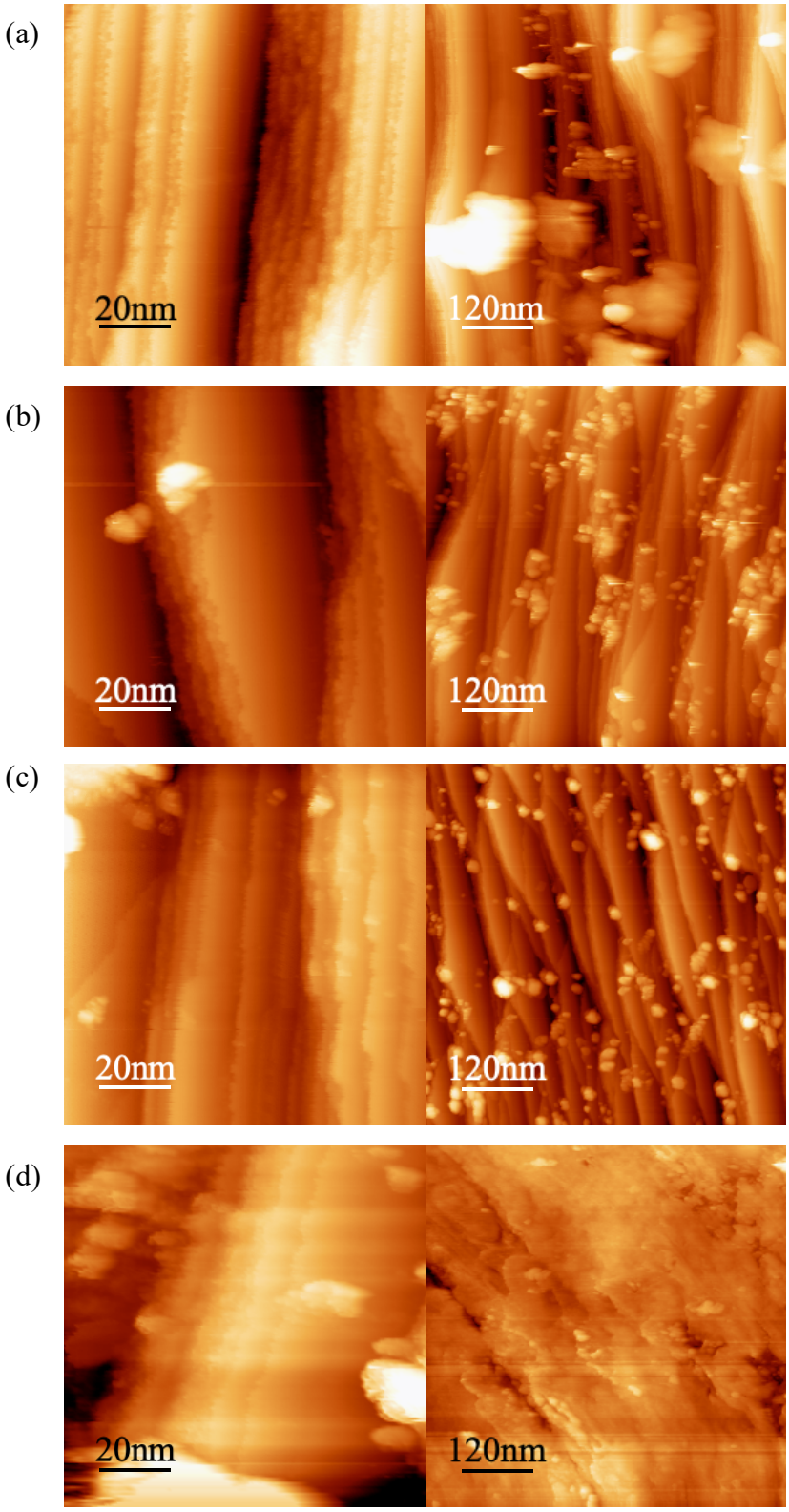

Fig. 2.6 UHV-STM topographies on the vicinal silicon surface after DC flash durations of (a) 20 sec, (b) 30 sec, (c) 180 sec, and (d) 1.5 h. Scan areas (Right)100 x 100 nm^2, (Left) 600 x 600 nm^2 (constant current mode, 1.7 nA, 2.1 V)

From these comparisons, it can be deduced that the duration of the flash needs to accumulate enough thermal energy to decompose any surface contaminants and oxide layer. At the same time, it is not feasible to apply a simply longer duration of DC flash because of the surface contamination speculated to be due to degassing from the sample holding fixture in the experimental setup.

2.3.3 DC flash energy dosage dependence

In order to accumulate more thermal energy to the sample while keeping the sample holder fixture at a relatively lower temperature to avoid degassing, it is effective to apply the number of intermittent DC flashes. The intention is to keep the single duration of DC flash not to exceed 30 sec where the degassing effect was minimized as suggested from the study in the previous section, as well as to accumulate the total energy dosage by multiple numbers of DC flashes.

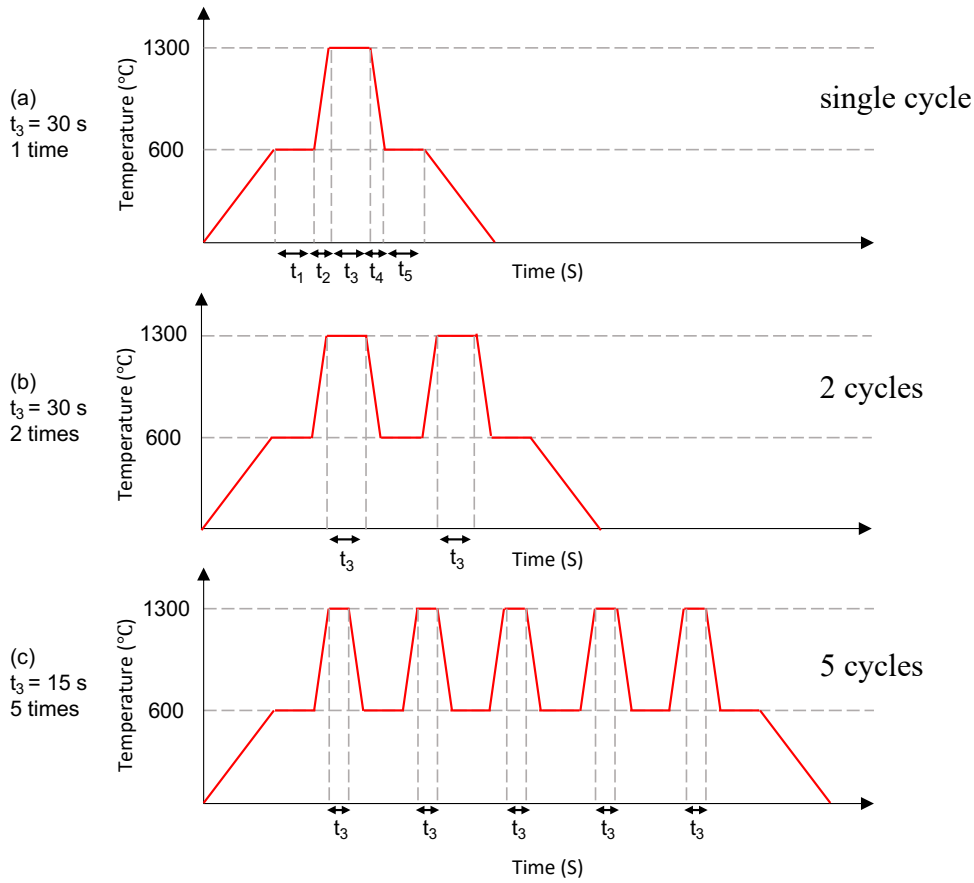

Fig. 2.7 DC flash cycle diagram corresponding to the measurements shown in Fig. 2.6

The overall DC flash procedure is shown in the diagram in Fig. 2.7. The sample is first warmed up to 600 °C keeping the pressure under 1×10^{-9} mbar. Once the chamber pressure is stable (t_1 depends on the sample), the DC current is applied quickly to achieve 1300 °C (t_2), and then kept for either t_3=30 or 15 sec, for sample (a), (b), and (c) respectively. For each DC flash, the highest temperature at the sample surface was measured to be 1200-1300 °C. Between the intermittent DC flash procedure, the sample surface was cooled down to 600 °C (t_4), and kept for *ca.* 1 min to release the thermal stress on the sample holder fixture (t_5), and then gradually turned off over *ca.* 1 min. The vicinal angle of the sample is the same as in the previous section, namely 3°.

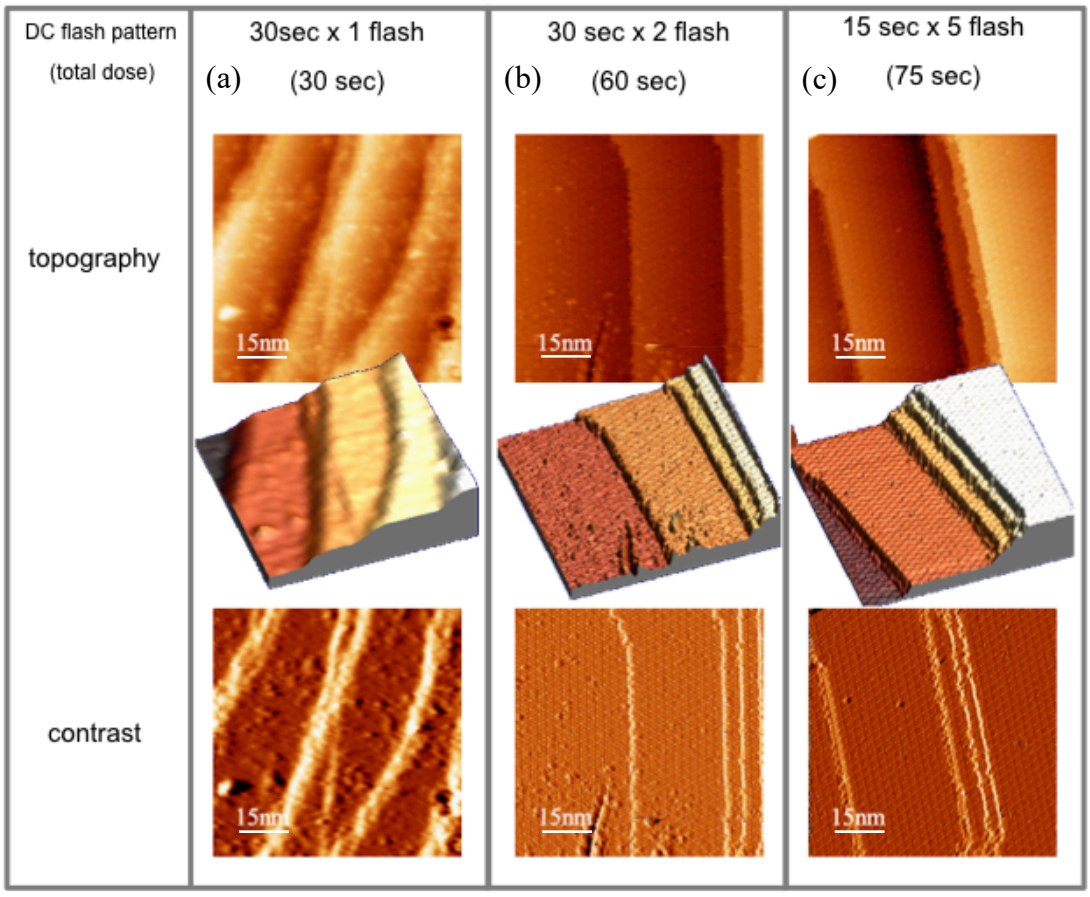

Fig. 2.8 DC flash energy dose dependency (a) DC flash for 30 sec x single cycle (b) 30 sec x 2 cycles (c) 15 sec x 5 cycles (constant current mode, 1.4 nA, 1.6 V)

Fig. 2.8 (a) shows the sample surface after three different DC flash procedures. After 30 sec total duration (30 sec x single-cycle flash), the UHV-STM image shows relatively low contrast and some contaminations on the surface.

After another 30 sec of flash (30 sec x 2 cycles flash, total 60 sec duration), the sample surface showed fewer contaminants and exerted significantly sharper topo-

graphic image with the Constant-Current mode imaging, which indicates the higher conductance due to better order on the surface. The step edge morphology was also sharper and well-ordered compared to previous patterns of DC flash procedure, but in the area under investigation.

Different DC flash pattern was performed to identify if the number of repetitive flashes is critical to reducing the surface contaminants while keeping the total duration in a similar amount. Applying 15 sec x 5 cycles flashes (total dosage 75 sec) exerted somewhat better surface quality in both contaminants and the step edge morphology. However, the difference was not prominent.

From these comparisons, keeping the sample surface at 1200-1300 °C for the total duration above 60 sec results in clean surface quality with atomic step edges and terraces.

This atomically clean surface preserving bilayers was observed after multiple flashes in the above samples. Fig. 2.9 shows the multiple layers of steps on the silicon surface after 30 sec x 2 cycles DC flash. The terraces of the steps exerted the superstructure of Si(111)-7x7 reconstruction. Moreover, from the UHV-STM topography, each step is identified to be monoatomic layers on (111) surface, which has *ca.* 0.3 nm, as indicated in Fig. 2.9 (d). [6] The superstructure of the Si(111)-7x7 reconstruction shall be discussed in the subsequent section.

From this observation, it is concluded that the multiple numbers of intermittent DC flash procedures are effective in obtaining a clean silicon surface, reserving the step edges for some extension of the area on the surface. The multiple intermittent DC flash conditions are that; each time less than 30 sec, and more than 2 cycle repetition, total duration accumulates more than 60 sec.

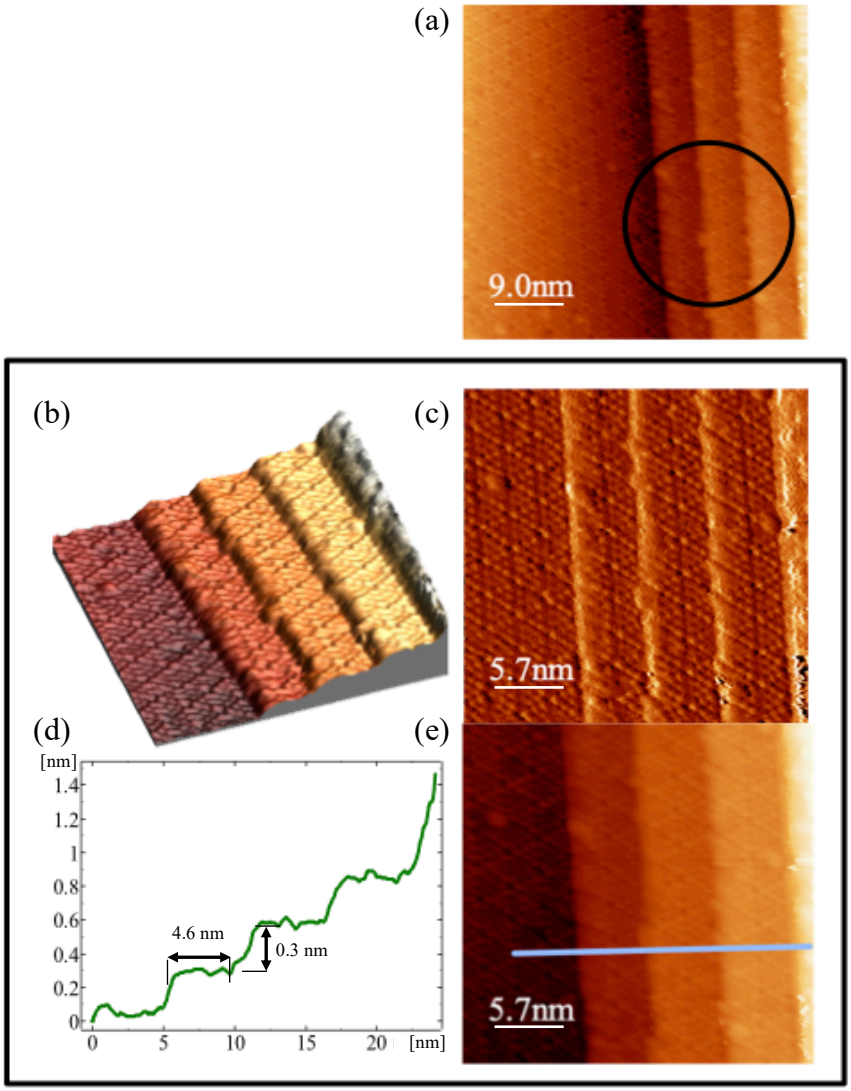

Fig. 2.9 atomic steps of Si(111) stepped surface after 30 sec x 2 cycles flash. 7x7 reconstructed superstructure can be seen on the steps. Single unit per each terrace, indicates the surface energy minimization by lining up the corner holes of 7x7 unit cell. 0.3 nm height profile of a single step confirms the bilayer of Si(111) (ref. Fig. 3.1). The area indicated by circle in (a) is enlarged in (b) 3D image, (c) contrast image, and in (d) height image. (constant current mode, 1.4 nA, 1.6 V)

2.3.4 Vicinal angle dependence on the vicinal silicon surface

The bilayer atomic steps and terraces without significant surface contamination were observed in most of the scanning area. However, to utilize such a surface as a building block for further studies, the surface conditions have to exert such steps and terrace structure over substantially long range, which is enough to observe the two-dimensional superstructure of the organic molecules, with reasonable reproducibility.

Fig. 2.10 shows the example of wider area observation on the identical sample from Fig. 2.9, which exerted the bilayer atomic steps with a clean surface on several sampling points. Despite the ordered morphology on the local scanning area, *i.e., ca.* 10 x 10 nm^2 range, the wider area (300 x 300 nm^2) showed aggregated layers of steps without long-range order on the step edges. This confirms the limited extension of the step edge order.

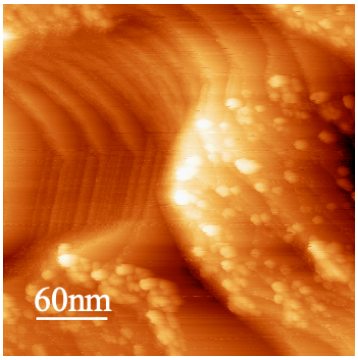

Fig. 2.10 Wider area observation on the identical sample from Fig.2.9. Scanning area 300 x 300 nm^2 (constant current mode, 1.4 nA, 1.6 V)

The aggregated steps on the surface on a wider range can be explained by the nature of the vicinal angle on the surface.[19] This sample has the vicinal angle of 3°, which means the average terrace width in theoretical expectation is *ca.* 5.7 nm considering the atomic bilayer height being 0.3 nm (0.3 nm / tangent 3° = 5.7 nm). Thus, lower vicinal angles are expected to exert wider terraces, which gives more probability for the step edges to extend without step bunching or alternation.

The purpose of this Study is to obtain a surface structure that is suitable for the organic molecule superstructure with respect to the step edges, which shall be the building block for future device application. Thus, it is important to reproduce the atomically straight step edges at least for several hundred nm of straight steps, apart from each other.

To confirm the vicinal angle dependence on the separation of the step edges, the Si(111) wafer with 0.35° nominal miscut was chosen for further study. 0.35° of miscut angle shall provide *ca.* 49 nm of bilayer atomic terrace (0.3 nm / tangent 0.35° = 49 nm).

Fig. 2.11 shows a comparison between 3° and 0.35° nominal miscut angles of silicon wafers. Both wafers were purchased from Silchem GmbH, Germany. The DC flash procedure is; t_3= 180 sec, single cycle DC current parallel to the step edges. The 0.35° nominal miscut surface exerted significantly wider terrace areas, resulting from the well-separation of the step edges. Most of the layers on the steps are bilayers, which is confirmed from the direct measurement of step height by UHV-STM topography. The miscut angle as low as 0.35° on the vicinal silicon surface plays a critical role in obtaining the atomically flat steps and terraces.

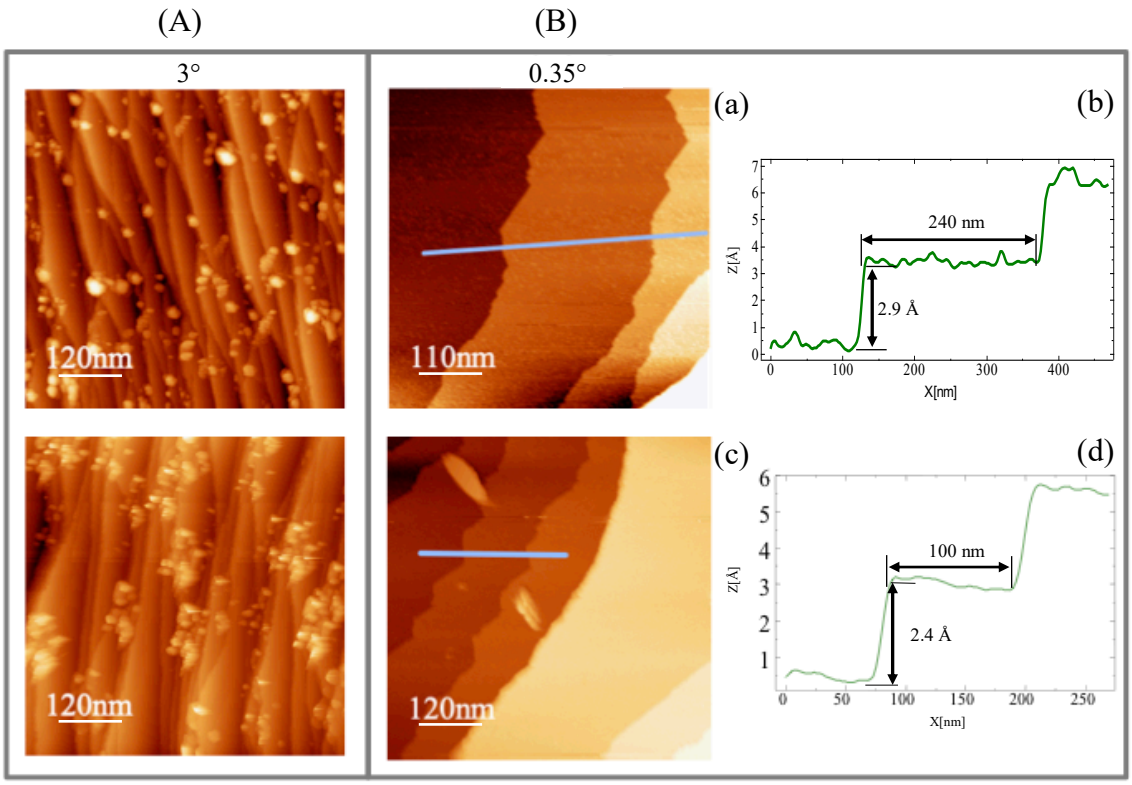

Fig. 2.11 Comparison between (A) 3° miscut and (B) 0.35° miscut Si (111) surface topography. (B) 0.35° surface exerted wider separation of the step edges, without step bunching effect, in comparison to (A). Scanning area (a) 550 x 550 nm^2 (c) 600 x 600 nm^2. (b) and (d) show the height profile along the indicated lines in (a) and (b), respectively. The height profile confirms the monoatomic step of Si(111) layer.

Fig. 2.12 shows the sample surface after 30 sec x 6 cycles of DC flashes, parallel to the step edges, on the 0.35° miscut angle silicon surface. Throughout the process, the chamber atmosphere is kept 1×10^{-9} mbar. The samples from this preparation procedure exerted very clean surfaces over a few mm range. There is no significant contamination observed under the single scan area. Even after moving the scan area for more than a few millimeters apart, the sample also showed a similarly clean surface. The straight step edges are also observed for more than several hundred nm extensions.

(a)

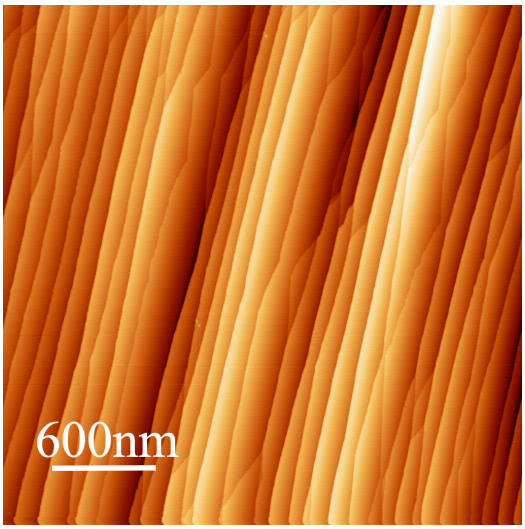

(b)

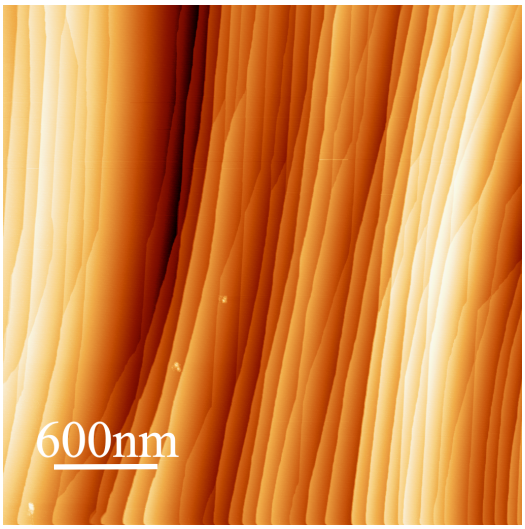

(c)

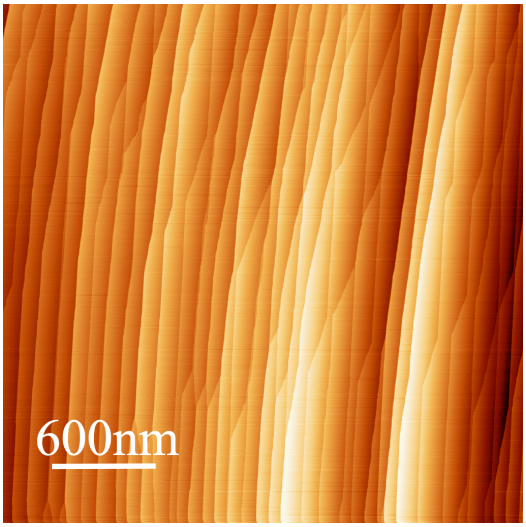

Fig. 2.12 UHV-STM topography (constant current mode, 1 nA, 2.1 V) on Si(111) 0.35 º miscut angle, after 30 sec x 6 cycles, DC current parallel to the step edges. (a), (b) and (c) are from three different scanning locations from an identical sample. Each location is separated from each other for more than a few millimeters, which confirms clean and homogeneous surface condition over significantly wide area. Scanning area 3000 x 3000 nm^2.

Fig. 2.13 shows a detailed scan of the step edge structure. The unilateral step edges can be found without significant kinks. The surface cleanliness is also confirmed from the observation of several points on the terraces. It is also confirmed that the step with Si(111)-7x7 unit cell aligned for more than a hundred nm range in many of the scanning areas.

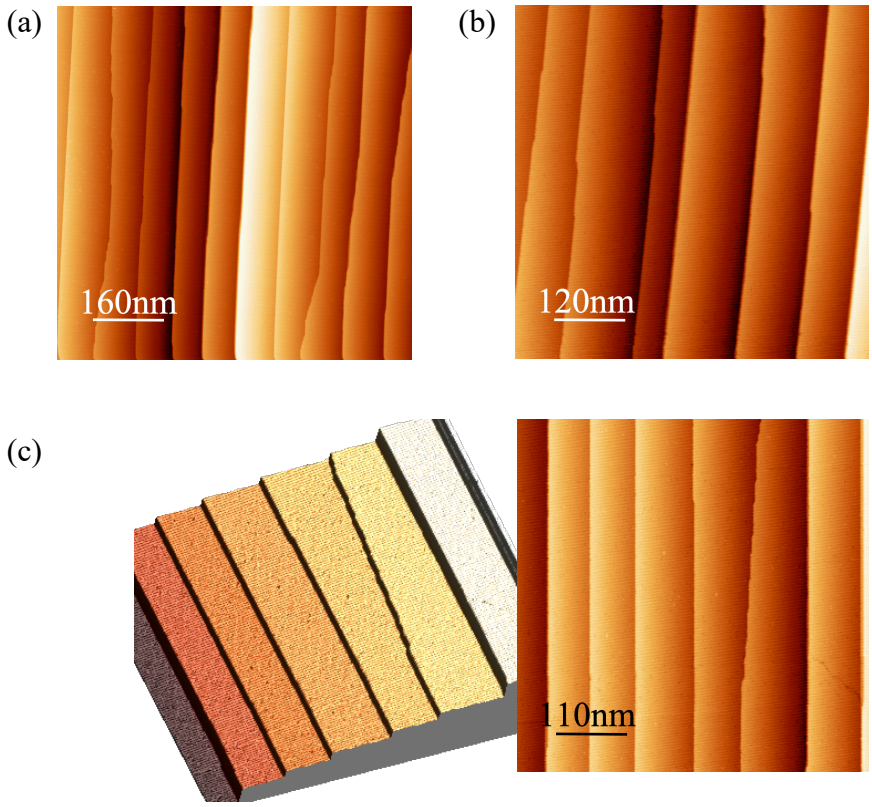

Fig. 2.13 Three different locations observation on the step edges. Distinct edge structure can be found. The 3D topography illustrates that the number of atomic layers may differ on the steps. Scanning area (a) 800 x 800 nm^2 (b) 600 x 600 nm^2 (c) 550 x 500 nm^2. (constant current mode, 0.5 nA, 3.0 V)

As to the bilayers and the atomic superstructure on the terraces, Fig. 2.14 confirms the distinct Si(111)-7x7 surface reconstruction, as well as the discrete atomic layers, in this case, three layers at a step edge. These are typical surface features on the sample prepared in the same manner in this Study.

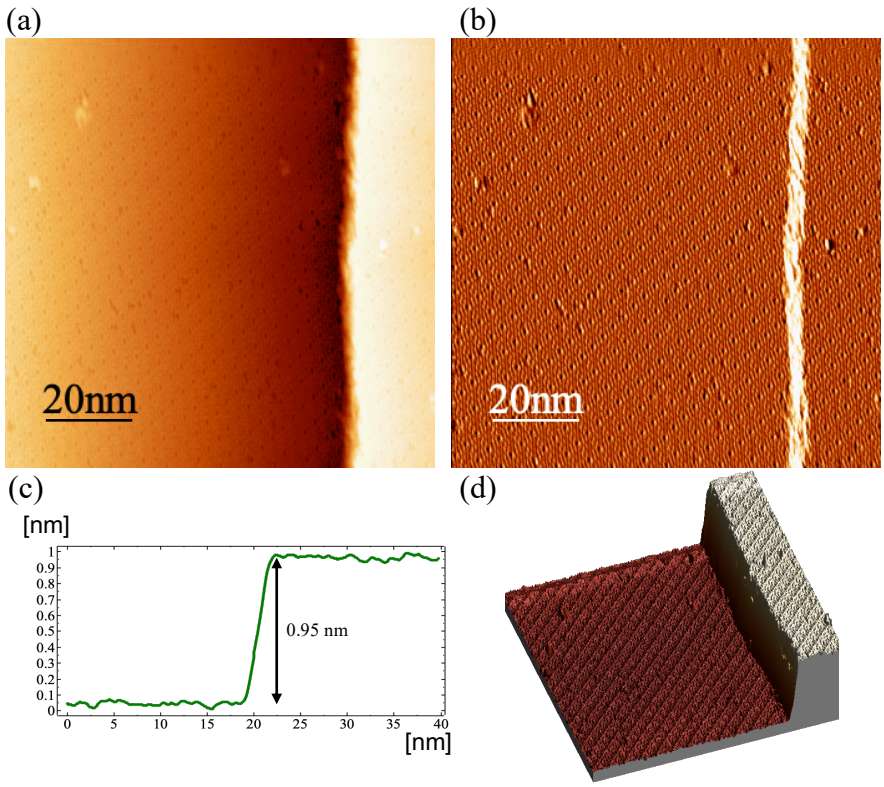

Fig. 2.14 Typical sample surface at 20 nm^2 scan range observation. Distinct feature of Si(111)-7x7 surface reconstruction can be observed. The step edge is consisted of 3 bilayers on this step. (a) height image (b) contrast image of the same data. The Si(111)-7x7 reconstruction structure are more visible. (c) height profile of the step. Considering the height of bilayer 0.3 nm, this step shows *ca.* 3 bilayers. (d) 3D representation of (a). (constant current mode, 2.0 nA, 2.2 V)

The above findings agree with preceding studies made by *Himpsel's* group in their study of the stepped structure on the vicinal silicon surface. [19, 6] In their study, lower miscut angles are, in general, said to preserve bilayers at the steps. It also showed the thermal procedures giving rise to morphological alternation. These discussions coincide

with the finding of this Study.

2.3.5 Surface reconstruction and the symmetry with vicinal surface

In terms of the surface reconstruction, the Si(111)-7x7 surface atomic configurations possess distinct arrangements proposed by *Takayanagi et al.,* depicted in Fig. 2.15. [56]

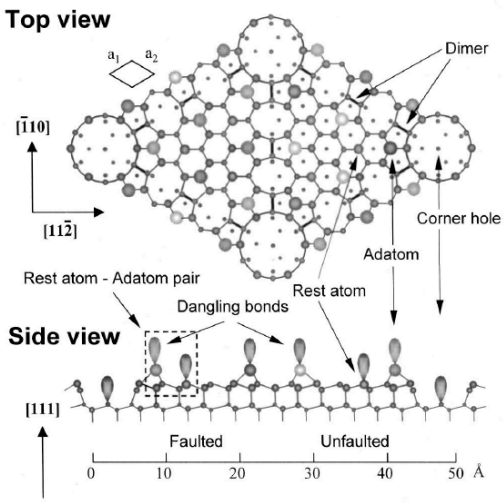

Fig. 2.15 Dimer-adatom-stacking fault (DAS) model of Si(111)-7x7 unit cell proposed by *Takayanagi et al.* [56] Reproduced from *Cao et al.* [81], with the permission of AIP Publishing.

The detailed STM topography confirms the distinct feature of Si(111)-7x7 reconstructed superstructure, as shown in Fig. 2.16 and Fig. 2.17. The images are taken in the middle of a terrace of the sample surface with a miscut angle of 0.35° after the DC flash process described in the previous section, namely 30 sec x 6 cycles, DC current parallel to the step edges.

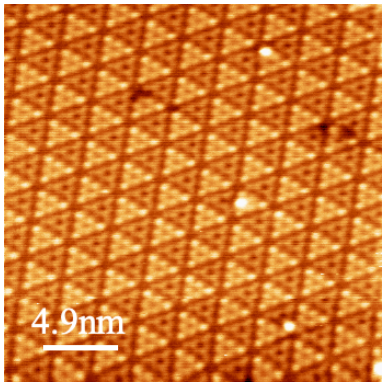

Fig. 2.16 STM topography on a terrace. The distinct superstructure of Si(111)-7x7 can be observed. Scanning area 24.5 x 24.5 nm^2. (constant current mode, 2.0 nA, -2.0 V)

(a)

(b)

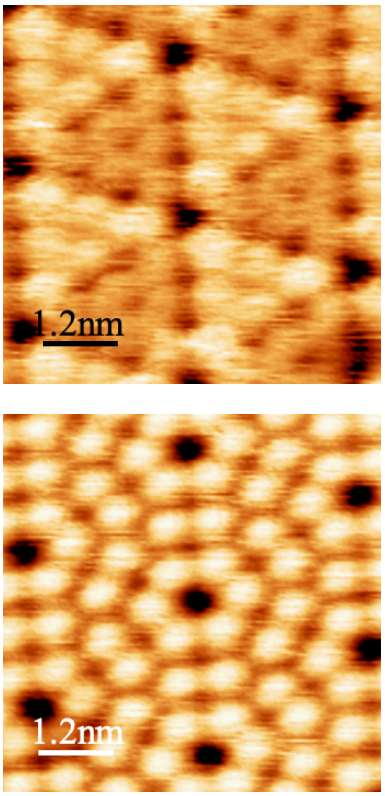

Fig. 2.17 STM topography on Si(111)-7x7 surface observed on a terrace by constant-current mode at 2.0 nA, (a) sample bias -2.0 V, (b) +2.2 V. Scanning area 6 x 6 nm^2 for both images. Different electronic states are observed by varying the sample bias voltage.

In Fig. 2.17 (a), with the sample bias voltage at -2.0 V, the darker triangle and the brighter triangles are observed. This contrast is due to the difference in the local density of state between the rest atom-adatom pair on the faulted side and the unfaulted site, as depicted in Fig. 2.15. By varying the sample bias voltage to +2.2 V in Fig. 2.17 (b), the image shows only the topmost surface adatom configurations.

The surface superstructure is also confirmed by means of the low energy electron diffraction (LEED) technique to identify the symmetry of the surface atomic arrangement. A commercially available LEED setup is employed in this Study (SPECTALEED by Omicron Vakuumphysik GmbH).

Fig. 2.18 (a) shows the LEED patterns on the sample before the DC repetitive flash procedure, where the surface oxide layer is anticipated to prevail. It confirms the three-fold symmetry in rotation on the Si(111) surface.

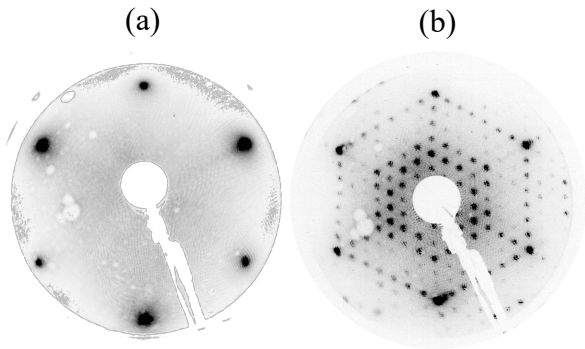

Fig. 2.18 LEED patterns obtained from (a) silicon(111) surface before repetitive DC flash procedure (b) after DC flash procure and STM observation. Both taken with beam energy at 36 eV.

This corresponds well to the theoretical calculation of the LEED pattern on the Si(111) surface. Fig. 2.19 depicts the schematic of the LEED configuration, which is simulated in this Study. The dimension of the experimental setup was referred to from the machine specification by Omicron Vakuumphysik GmbH. The assumptions in the simulations are; elastic collision, spherical wavefunction reflection, no shading-effects. In order to simulate the effect of long-range order and the contrast on the LEED pattern, two different numbers of atoms in the system are simulated, *i.e.,* 184 and 536. 184 atoms in the simulated system represent less order in the surface structure compared to the one with 536 atoms. In both systems, the topmost bilayer on Si(111) surface is reproduced in the simulation without surface reconstruction as depicted in Fig. 3.1. Namely, the topmost surface structure of Si(111) is 1x1.

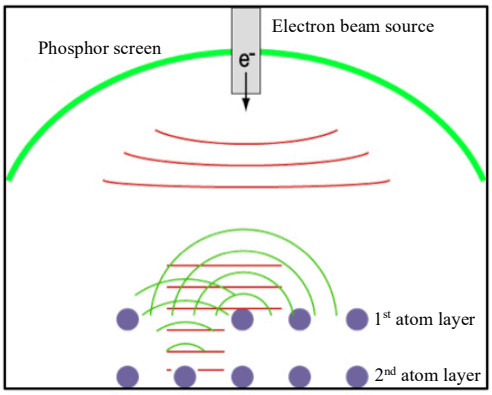

Fig. 2.19 Schematic of the LEED simulation configuration. Electron beam wavefunction is reflected by the elastic collision with surface atoms. The scale in the represented schematic is not proportional to actual dimension.

The simulated LEED patterns are shown in Fig. 2.20 at the beam energy of 48 eV. The patterns coincide well with the experimental results. The three-fold symmetry in rotation can be observed both in the experiment (Fig. 2.18 (b)) and the simulation (Fig. 2.20 (b)). It is also worth noticing the contrast of the spots in the simulation is sharper when the number of atoms in the simulated system is larger. Namely, Fig. 2.20 (b) exerts blur spots than Fig. 2.20 (d). This effect is also observed in the actual experimental results on the various samples where the spots in the LEED patterns are a blur. Less surface cleanliness is anticipated by the slight increase of the pressure in the UHV chamber during the experimental procedures.

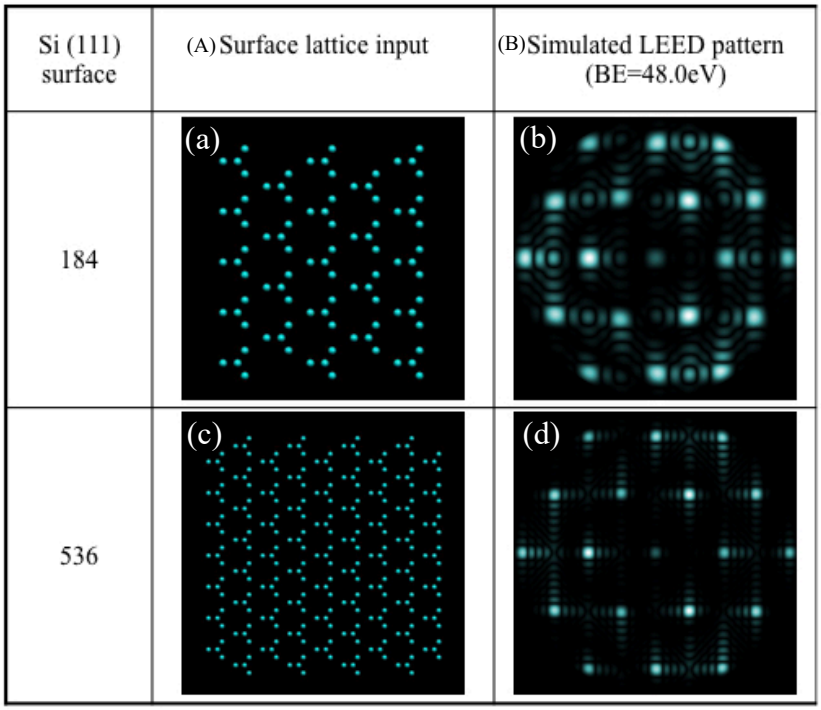

Fig. 2.20 Simulated LEED patterns on the Si(111)1x1 surface. (A) silicon surface atom configuration input for the simulation (B) simulated LEED patterns at the beam energy of 48 eV. The number of silicon atoms in the simulation is (a) 184 and (c) 536. (c) 536 atoms represent the surface lattice order in longer extension, compared to (a) 184 atom system.

From the above studies, the atomically straight step edges and flat terraces are obtained by utilizing 0.35° miscut Si(111)-7x7 reconstructed surface when applied a proper DC flash procedure. The surface cleanliness and structural order prepared in this manner are maintained over the area as large as the sub-micrometer range. The surface prepared in this manner can serve as an ideal substrate for further study to examine if organic molecules can form low dimensional structures.

2.4 Summary

The clean Si(111)-7x7 reconstructed vicinal surface is obtained for the intention to utilize as the base substrate for the further purpose of this Study. In terms of the topography of the steps and terraces, the vicinal angle is of most importance. In this Study, 0.35° miscut is confirmed to be suitable. The sufficient surface cleanliness and the straightness of the step edges are achieved by optimizing the DC flash procedure, which in this case, intermittent flashes each time 30 sec and repeat for 6 cycles, followed by the gradual cooling process. The resulting process is in alignment with the process that was previous reported in a similar system. [19, 6] The total duration of the DC flash procedure impacts the residual surface contaminants' amount. However, having less critical importance once the clean surface is obtained after a sufficient amount of energy to construct Si(111)-7x7 superstructure.

3 Self-assembly of CuPc molecules on hydrogen passivated and clean vicinal silicon surface [58]

3.1 The motivation

Controlling the conformation of organic molecules on inorganic semiconductor surfaces is of interest in the light of material science and novel device applications, *e.g.,* for organic/inorganic hybrid devices.

The vicinal silicon surface is one of the promising candidates as a template for structuring organic molecules by using the self-assembly method. Utilizing the atomic steps and terraces on the vicinal surface, aggregation of organic molecules at the step edges can lead to one-dimensional molecular structures on the vicinal silicon surface. [6, 22]

On the other hand, copper-phthalocyanine (CuPc) has attracted much attention as one of the most widely used organic molecules, *e.g.,* as active layers in organic thin-film transistors [59, 60] and organic light-emitting devices [61]. When the organic molecule is employed in the active layer of optoelectronic devices, control of the molecular orientation in thin films becomes an important issue because of the anisotropic properties of the single CuPc molecule. [16, 62, 63, 64]

CuPc and Si(111)-7x7 surface, however, is reported to exert strong chemical reactivity, suggesting strong local binding at the landing site when CuPc is directly deposited on a clean Si(111)-7x7 substrate. [65] To induce the self-assembly of CuPc, the surface reactivity of Si(111)-7x7 needs to be deactivated. Hydrogen passivation is expected to provide such a deactivated surface by capping the dangling bonds on the Si(111)-7x7 surface. The intention of H passivation in this Study is two folds. The first is to deactivate the surface dangling bonds on Si(111)-7x7 reconstructed surface, where 19 dangling bonds exist per reconstructed unit cell. [56, 66, 67] Second is to preserve the atomic flatness of the steps and terraces on the vicinal surface, even after the passivation process.

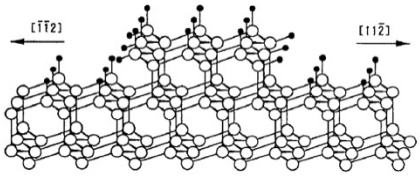

Fig. 3.1 A side view of Si(111) around step edges. A step edge consists of two atomic layers *i.e.,* bilayers of crystal structures. The dangling bonds on the terraces and the step edges in Fig. 1.3 are terminated with hydrogen as depicted in this model. Reproduced from *Kaji et al.*[82], with the permission of AIP Publishing.

3.2 Experimental

3.2.1 Si(111)-7x7 substrate preparation

(111) oriented silicon wafer material with natural oxide was supplied by Silchem GmbH, Germany. The surface has a nominal miscut angle of 0.35° with respect to $[111]$ surface normal. The miscut angle is tilted towards $[1\bar{1}0]$ direction and the step edges are

thus parallel to the primary flat of the wafer. The wafer was cut into strips with a dimension of 1.0 x 15 mm^2. The cut silicon strips were mounted on the sample holder that is capable of direct current heating, *i.e.,* current passes through the silicon strip so that the silicon can be directly heated up to high temperatures. The silicon strip was mounted on the sample holder in a direction such that the current flows parallel to the step edges. After mounting on the sample holder, the samples were transferred into an ultra-high vacuum scanning tunneling microscope (UHV-STM, Omicron GmbH Germany) chamber where the base pressure is lower than 2×10^{-10} mbar. In UHV, the samples were degassed by a conventional ceramic heater at 700 °C for over 12 h until the base pressure was recovered.

Direct current heating is then performed in order to desorb the natural oxide layer and form atomically ordered steps and terraces on the vicinal surface. The silicon strip was heated up to around 750 °C, then flashed to above 1200 °C for about 3 sec by rapidly increasing the current passing through the silicon strip. The current was then quenched to cool down the sample to the temperature range between 700 °C and 800 °C and annealed for 5 min so that the surface reconstruction and straight step edges can prevail to a large extent due to electromigration. After this surface preparation procedure, the silicon surfaces are known to possess a 7x7 reconstruction and atomically straight step edges and flat terraces. Elaborate studies on the preparation procedure of the vicinal silicon surfaces were presented elsewhere. [6]

3.2.2 Hydrogen passivation on Si(111)-7x7

After the preparation of the clean silicon (111)-7x7 surface, passivation with H

was performed in situ. Hydrogen gas (99.9999%) was introduced into the UHV chamber via a leaking valve where a tungsten filament was heated above 1500 °C to crack H_2 molecules into atomic hydrogens. The samples were facing the tungsten filament at an 8 cm distance during the exposure. The dose of the atomic hydrogen was equivalent to 3.6 L, with the pressure being 1.6×10^{-7} mbar. Almost full H coverage was indirectly confirmed by thermal desorption experiments afterward using UHV-STM. The dose of the atomic H was optimized to achieve the so-called "1st channel" reaction, which terminates the dangling bonds on the 7x7 reconstructed surfaces, preserving the surface reconstruction and the atomically flat terraces. [34] A different experimental geometry of the sample and the tungsten filament can account for the considerably lower dose of the atomic H needed for full coverage on the Si(111)-7x7 surface compared to that in a previous report (2.1 x 103 L). [34]

3.2.3 CuPc deposition

CuPc (sublimed grade (>98.5%), SynTec GmbH, Germany) was deposited by means of organic molecular beam deposition (OMBD) in the UHV chamber on two types of surfaces, *i.e.,* the H passivated, and the clean 7x7 reconstructed vicinal silicon substrates. CuPc was loaded into a thoroughly degassed molybdenum crucible. The crucible was then installed in a Knudsen cell and degassed overnight until the pressure was stabilized. The crucible was kept at 465°C during OMBD, which gave the deposition rate of 3.5×10^{-3} ML/s. The pressure remained below 5×10^{-9} mbar during the deposition.

CuPc was observed on three different types of surfaces. The first is on the H

passivated surface. The second is the identical surface after thermal desorption of CuPc. The third is on a clean Si(111)-7x7 surface without H passivation.

On the H passivated surface, CuPc was subsequently deposited onto the H passivated surface in steps until full coverage was achieved to monitor the evolution of CuPc growth on the H passivated vicinal silicon surfaces. The substrate was warmed up to 150 °C every time before CuPc deposition to have better self-assembly by higher molecular mobility. After the deposition, the sample was annealed at 150 °C for 2 min and then cooled down to room temperature before performing STM to reduce thermal drift effects. Second, to confirm the assumption that the H passivation is preventing the covalent bonding of CuPc to the dangling bonds on Si(111)-7x7, the identical sample was annealed at 546 °C for 30 min with the intention to desorb CuPc. Thirdly, CuPc was deposited afresh on another sample surface of vicinal Si(111)-7x7 in order to confirm the effect of H passivation.

All the images were obtained at room temperature with constant current mode. The imaging parameters were adjusted to achieve the highest contrast at each CuPc coverage.

3.3 CuPc topography observation with dose dependence on H-passivated Si surface

Fig. 3.2 shows the vicinal Si(111)-7x7 surface after the H passivation. The steps

and terraces are clearly observed. Every step was confirmed using height profiles to consist of a bilayer of silicon (0.3 nm). The terrace width in the image varies from *ca.* 3 to 9 x 10 nm. The 7x7 reconstruction was still observed after the H passivation in detailed scans (inset of Fig. 3.2) and also by means of low energy electron diffraction (LEED). Sufficient cleanliness was confirmed by STM and also by the significantly low background intensity in the LEED patterns.

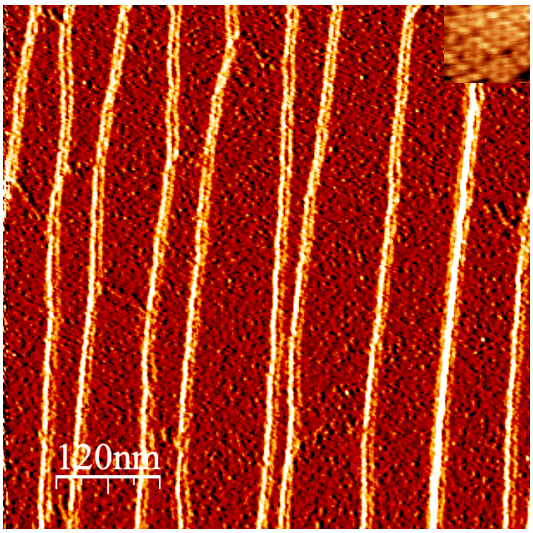

Fig. 3.2 High-pass filtered STM topography of an in situ hydrogen passivated vicinal silicon surface with 0.35° nominal miscut angle with respect to [111], tilted towards the $[1\bar{1}0]$ direction (dimension 600 x 600 nm^2, sample bias -1.6 V, tunnel current 0.27 nA). Inset: atomically resolved image on a terrace. The hydrogen passivated 7x7 unit cell can be observed. (6.7 x 7.0 nm^2, 0.50 nA, -1.4 V)

Fig. 3.3 shows a suggested model of CuPc with respect to a unit cell of Si(111)-7x7 reconstruction surface. The dimensions are deduced from the previous reports in order to estimate the order of CuPc dimensions with respect to the unit cells of Si(111)-7x7 reconstructed surface. [16, 56] From this estimated dimension, it is anticipated that a single CuPc molecule occupies almost half of a Si(111)-7x7 unit cell when lying flat on the surface.

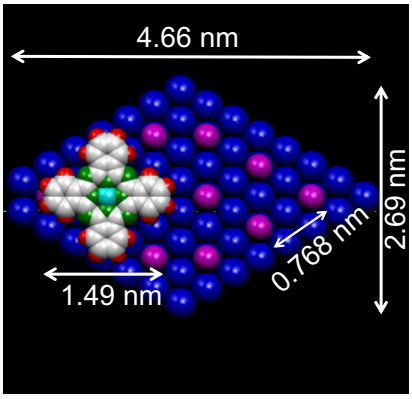

Fig. 3.3 A model of a single CuPc molecule on a unit cell of Si(111)-7x7 reconstructed surface. The dimensions are deducted from the previous reports in order to estimate the order of CuPc dimensions with respect to the unit cells of Si(111)-7x7 reconstructed surface. [16, 56]

CuPc was very sparsely deposited on this surface by exposing the surfaces towards the evaporation cell (0.035 ML). The monolayer coverage was derived from the area ratio between the substrate and total CuPc coverage in the STM images. Individual CuPc on a terrace is shown in Fig. 3.4. CuPc molecule is appearing as a bright spot that covers almost one-half of the H passivated 7x7 reconstruction unit cell. [68] This is in

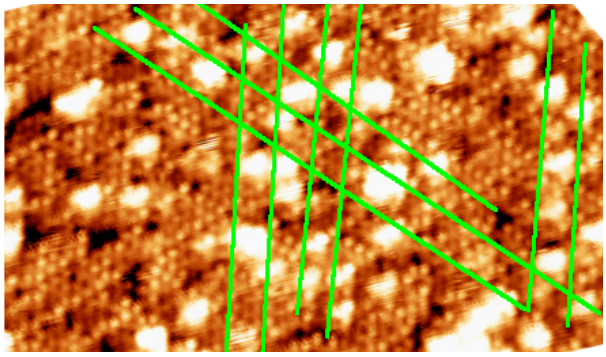

Fig. 3.4 CuPc on the hydrogen passivated Si(111)-7x7 surface (0.035 ML coverage). The green lines indicate the unit cell of 7x7 reconstruction underneath CuPc, which suggests the tendency of CuPc to occupy one triangular half of the 7x7 unit cell. (35 x 20 nm^2, 0.42 nA, -1.8 V).

agreement with the suggested model in Fig. 3.3, which suggests CuPc in the experiment are lying flat on the surface. In fact, *Nakamura et al.* reported that CuPc lays flat on H-Si(111) surface. [28] In Fig. 3.4, there is higher contrast on some of the CuPc in the image. This can be an indication of the vertical stack of CuPc, whereas less bright CuPc are single molecules.

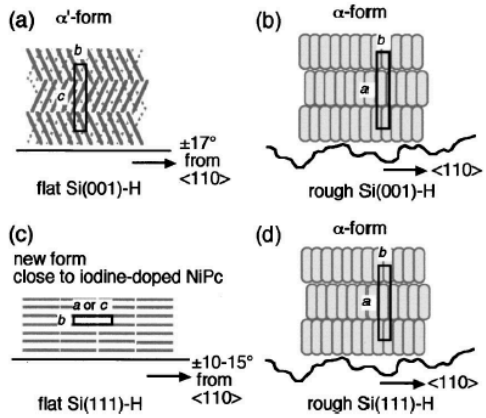

Fig. 3.5 *Nakamura et al.* reported various configuration of CuPc in-plane direction with respect to flat or rough surface condition. Reproduced from *Nakamura et al.* [28], with the permission of AIP Publishing. a-, b- and c-axis of CuPc crystallographic directions are indicated. These cited illustrations indicate the various types vertical stack of CuPc with respect to the substrate. The finding in Fig. 3.4 agrees with the model (c).

After subsequent deposition, 0.42 ML coverage, CuPc revealed a surprising growth behavior, as shown in Fig. 3.6. The STM images are taken again in the middle of a wide terrace.

It is surprising to find that CuPc started growing in an elongated linear structure on the terrace. Moreover, the direction of the elongation is parallel to the step edges, which are running along $[11\bar{2}]$ direction even though the step edges are at least 100 nm apart from the locations of the clusters of CuPc.

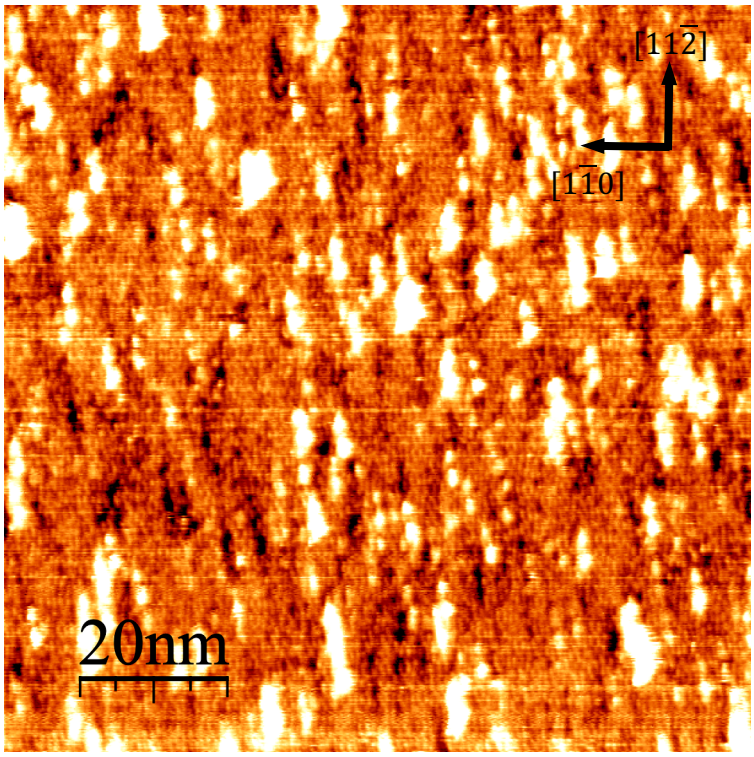

Fig. 3.6 After OMBD of CuPc (0.42 ML coverage) on the same sample as in Fig. 3.2 and Fig. 3.3. Clusters of the molecules elongated in vertical direction, which corresponds to parallel direction to the step edges. The scan area is chosen on a terrace without a step in the image. (100 x 100 nm^2, -1.4 V, 0.11 nA)

The strongly oriented growth mode became even more pronounced with the higher coverage of 0.63 ML. Fig. 3.7 reveals lines of CuPc, which are all parallel to the step edge direction. In order to exclude any thermal drift effect, which usually provides elongated structures in STM images, Fig. 3.7 was scanned with an azimuthal rotation of 45°. Since the elongated structures are still clearly observable towards $[11\bar{2}]$ direction with the different scan angles, artifacts due to thermal drift can clearly be excluded. This finding of linearly aligned CuPc is contrary to the previous report on a similar system, which showed three-fold symmetry of CuPc arrangement on Si(111) surface. [16, 29]

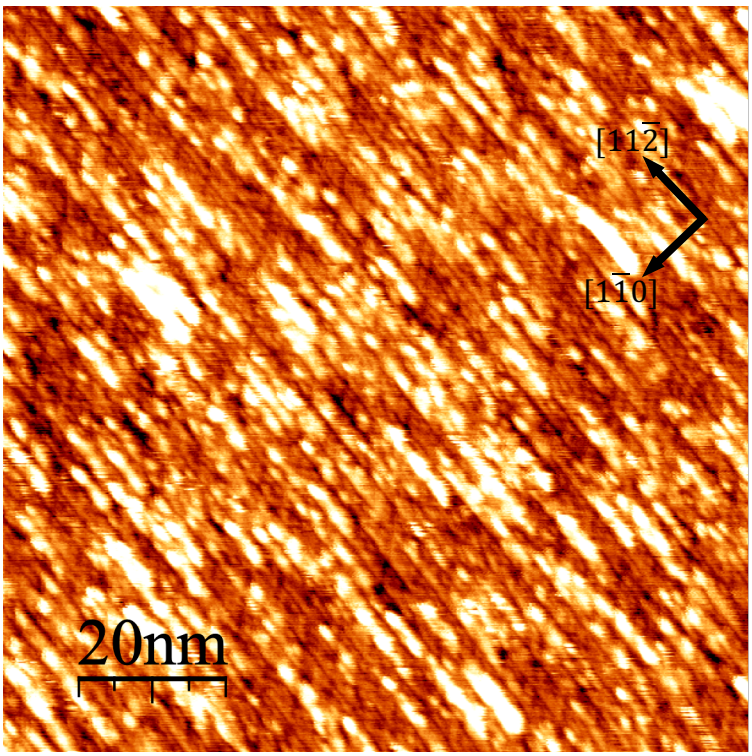

Fig. 3.7 After subsequent deposition of CuPc (0.63 ML coverage). The CuPc clearly self-assemble into elongated one-dimensional structures, diagonal in this picture from top left to bottom right (100 x 100 nm^2, -1.7 V, 0.067 nA)

When CuPc coverage becomes closer to full coverage by the nominal total deposition of 1.05 ML, the elongated structures result in long lines of the molecules covering a large area over the steps and the terraces (Fig. 3.8). The lines are strongly oriented parallel to $[11\bar{2}]$ direction. Though the step edges beneath CuPc are not directly observable by STM, there are from *ca.* 3 to 10 step edges expected in this image, estimated from the average terrace width on this identical sample. It is clear from the evolution of the clusters starting from Fig. 3.4 that the lines of the molecules are not just an aggregation of the molecules along the step edges and that the one-dimensional growth mode occurs on the

terraces isolated from the step edges resulting in dense lines of CuPc all parallel to the step edges.

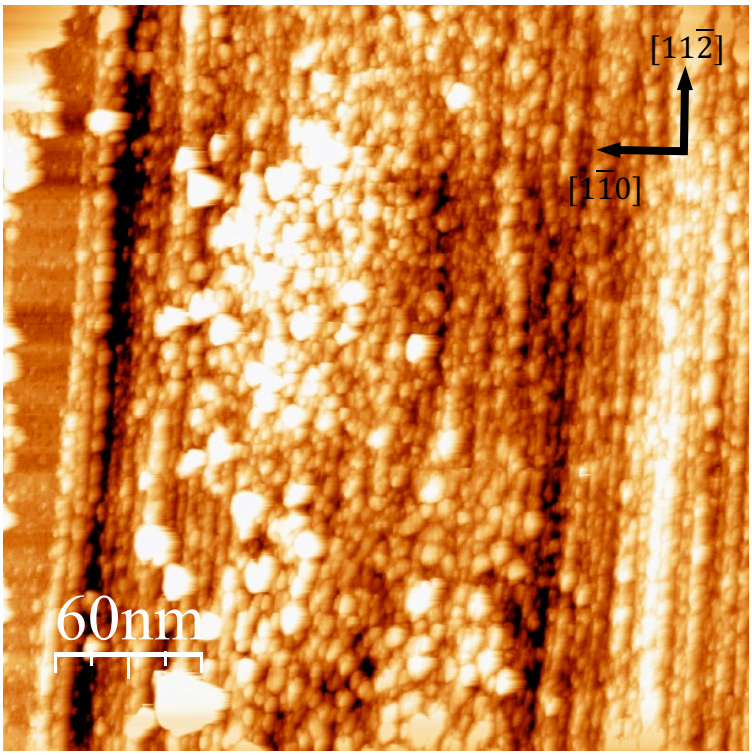

Fig. 3.8 Close to full monolayer coverage of CuPc on the hydrogen passivated vicinal silicon surface (1.05 ML coverage). one-dimensional growth of CuPc parallel to the step edges is clearly observed all over the terraces and the step edges. The number of lines of CuPc is larger than that of the step edges in the picture (300 x 300 nm^2, +1.4 V, 0.10 nA).

Moreover, the average width of a single terrace is 50 nm. Thus, the density of the lines of CuPc is much denser than the density of the step edges on the surface, justifying that the one-dimensional growth mode is not only due to the aggregation of the molecules at the step edges.

3.4 Thermal desorption of CuPc from hydrogen passivated Si(111)-7x7

In order to confirm the assumption that the H passivation is preventing the covalent bonding of CuPc to the dangling bonds on Si(111)-7x7, the identical sample from Fig. 3.8 was annealed at 546 °C for 30 min with the intention to desorb CuPc.

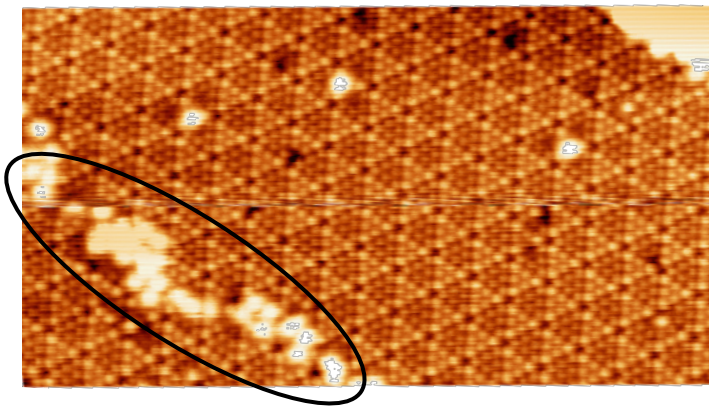

Fig. 3.9 Identical sample of Fig. 3.8 after annealing at 546 °C for 30 min. Image is taken on the location in the middle of a terrace between the steps on the vicinal surface. CuPc which covered almost a full monolayer are now desorbed, confirmed by the reappearance of Si(111)-7x7 reconstructed surface. Some CuPc are left attached to the surface which is indicated in the circle at bottom left of the image. (21 x 38 nm^2, 0.1 nA, -1.8 V)

Fig. 3.9 is the scanned image in the middle of a terrace between the steps after the annealing. On the contrary to Fig. 3.8 where CuPc covers almost full monolayer, it is confirmed that CuPc is desorbed after the annealing procedure, which supports the original intention of this Study that H passivation is vital to lower the binding energy between CuPc and the Si(111)-7x7 substrate. Some CuPc are left attached to the surface, which is indicated in the circle at the bottom left of the image. Although CuPc are aligned in a wire-like structure, this is not due to the aggregation to the step edge, as can be confirmed from the same height profile of the substrate around CuPc.

3.5 CuPc deposition on clean Si(111)-7x7 surface

In order to confirm the H passivation is critical for CuPc to form self-assembly, CuPc was deposited on a clean vicinal Si(111)-7x7 surface. As a result, it is confirmed CuPc did not form any ordered structure as this Study expected. (Fig. 3.10) The adsorption sites are rather random, and there is no indication for the elongated structure that was observed on the H passivated surfaces. This finding also supports the earlier report on the chemical bonding between CuPc and clean Si(111)-7x7. [65] Thus, it is concluded that the surface deactivation by passivation on the vicinal Si(111)-7x7 is playing an important role in reducing its interaction with the molecule and increase the molecular mobility on the surface.

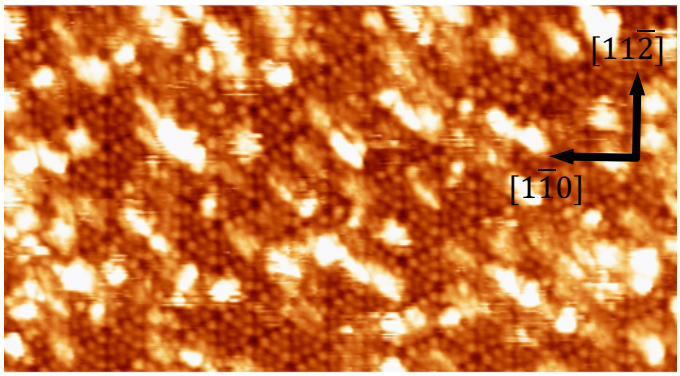

Fig. 3.10 A sub-monolayer coverage of CuPc deposited on the clean vicinal Si(111)-7x7 (0.42 ML coverage). There is no one-dimensional growth mode observed. (38 x 24 nm^2, 1.7 nA, -1.4 V)

The one-dimensional growth mode on the H passivated vicinal surface can be explained using the surface mass transport model, which was proposed by *Schwoebel et al.* [68], and later elaborated in detail, especially with organic molecules. [69] The diffusion

barrier height of the CuPc molecule is different between two directions, normal and parallel to the steps due to the edge height, which could have induced the oriented growth on the terraces.

Therefore, the growth mode of CuPc in the first few monolayers can be controlled by utilizing the H passivated vicinal silicon surfaces. Surprisingly the one-dimensional growth mode of CuPc starts in the middle of a terrace even when a cluster of the molecules is isolated from the nearest step edges. This elongated growth mode continues till the full coverage and forms a strongly oriented one-dimensional molecular structure, resulting in strong structural anisotropy.

3.6 Summary

The one-dimensional growth mode on an H passivated vicinal silicon (111) surface is confirmed. The original purpose of this Study anticipated some extent of one-dimensional growth of CuPc along the step edges of the vicinal silicon surface. Surprisingly, the one-dimensional growth is induced on the terrace where the CuPc absorption site is located apart from the step edges of the vicinal surface. The one-dimensional growth mode is confirmed to continue even more than the full molecular layer coverage of CuPc on this surface. From the finding that CuPc on clean Si(111)-7x7 without H passivation does not exert the one-dimensional growth mode, it is concluded that the surface interaction forces play an important role in the formation of the one-dimensional superstructure.

Since the single CuPc possesses strong optical and electronic anisotropy, this conformational anisotropy of CuPc in the thin film also induces a strong optical anisotropy. [63, 64] This controlled anisotropic property of organic molecular thin film using the vicinal silicon surface is promising in the light of organic/inorganic hybrid device applications.

4 Antimony passivated vicinal silicon surface and CuPc thin film [70]

4.1 The motivation

Despite the successful results in the earlier Chapter of this Study, the H passivation on the silicon surface requires careful preparation and analysis, mainly due to the experimental setup for the molecular H_2 cracking into atomic hydrogen [36], the handling of the hydrogen sources. The objective of this Study is to prepare the atomically ordered stepped silicon surface while maintaining the low chemical activity on the surface to allow organic molecules to self-assemble. Thus, the requirements are two folds. The first is to deactivate the surface dangling bonds on Si(111)-7x7 reconstructed surface, where 19 dangling bonds exist per reconstructed unit cell. [56] The second is to preserve the atomic flatness of the steps and terraces on the vicinal surface, even after the passivation process.

When it comes to the potential industrialization, the total surface process effort should be considered from the practicality and how accessible the technique is to achieve the designated surface conditions by different process setups. The passivation by the atomic H leaves instability in the reproducibility in terms of the quality of the surface conditions. One reason is the thermal effect on the sample surface by the filament during the atomic H passivation process. The irradiation of the filament may raise the temperature on the sample surface. The raised surface temperature is reported to cause the devia-

tion in the H passivation quality. [34, 35, 37, 36] Another reason is the possible chemical reaction of atomic H etches surface by forming silane, which may alter the flatness of the surface, of which the degree of such effect deserves discussion. [38, 39, 36] In addition to these intrinsic challenges, the gaseous hydrogen requires controlled in-let with differential pumping technique to incorporate with the UHV-STM apparatus, which demands more effort in experimental procedures with reproducibility in a practical sense. When it comes to the potential industrialization of this method, the total surface preparation process should be assessed from the practicality and accessibility of the technique in order to achieve the designated surface conditions.

Antimony (Sb), however, amongst other elements, is a suitable candidate for the objective of this Study. Antimony has been shown to cover the silicon surface with a bilayer due to the stronger affinity between Sb-Si, than Sb-Sb interaction when deposited at certain surface temperature conditions. [50, 51, 52] Sb is a semimetallic solid material, with a vapor pressure of 1×10^{-9} mbar at 520 °C, with the melting point at *ca.* 630 ºC under atmospheric pressure, which meets the conditions for the process of this Study. [47, 49] Sb is also chemically inert and can be handled without inducing a chemical reaction

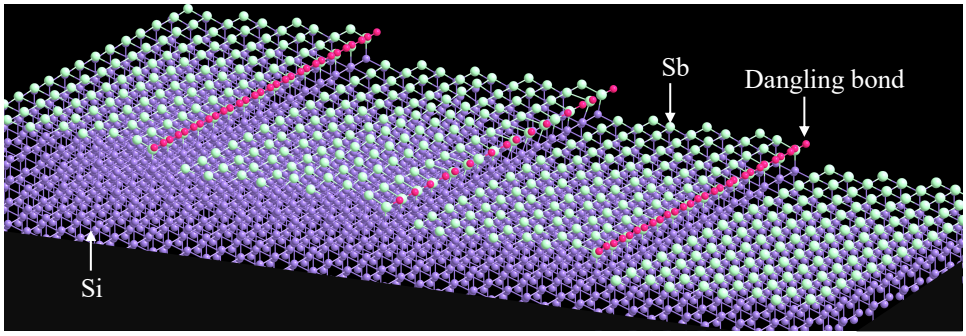

Fig. 4.1 A schematic model of Sb passivated Si(111) vicinal surface. The dangling bonds on the Si(111) terrace are terminated by Sb, while the step edge will leave dangling bonds due to geometric configuration.

in ambient conditions. Sb is reported to preserve the Si(111)-7x7 reconstruction surface [53, 54], or Si(111)-1x1 reconstruction [54] after passivating the dangling bond on the silicon surface. (Fig. 4.1) Whichever the case, the interface between adsorbed Sb atoms forms uniform coverage on the Si substrate, preserving the atomic structure of the Si surface bilayer. This is also important characteristics in the selection of the surface passivation technique in order to utilize the atomically configured silicon vicinal surfaces.

In this chapter, the Sb passivation on the vicinal silicon surface is performed and observed by means of UHV-STM. Subsequently, CuPc is deposited for sub-monolayer dose and observed. The UHV-STM observation on CuPc thin film on Sb terminated vicinal silicon surface has revealed a well-ordered island structure of CuPc thin film. What is more, a well-ordered columnar structure with multiple domains was formed on the islands of CuPc.

4.2 Experimental

4.2.1 Clean vicinal Si(111)-7x7 surface preparation

The vicinal silicon substrate was prepared in the same manner described in the previous chapter of this Study. The silicon wafer utilized in this chapter is the identical Si(111) wafer with a miscut of 0.35° titled from $[111]$ towards $[1\bar{1}0]$. The silicon strip was mounted on the sample holder in a direction such that the current flows parallel to the step edges. After mounting on the sample holder, the samples were transferred into the same UHV-STM, where the base pressure is lower than 2×10^{-10} mbar. In UHV, the samples were degassed by a conventional ceramic heater at 700 °C for over 12 h until the

base pressure was recovered. The same direct current heating procedure in the previous chapter of this Study is then performed in order to desorb the natural oxide layer and form atomically ordered steps and terraces on the vicinal surface. The silicon strip was heated up to around 750 °C, then flashed to above 1200 °C for about 3 sec by rapidly increasing the current passing through the silicon strip. The current was then quenched to cool down the sample to the temperature range between 700 °C and 800 °C and annealed for 5 min. By this preparation method, the vicinal silicon surface has been confirmed to have 7x7 reconstruction, as well as the atomically configured steps and terraces with atomic step heights.

4.2.2 Sb passivation

On this clean Si(111)-7x7 reconstructed surface, Sb is deposited by the conventional Knudsen cell thermal deposition technique. A commercially available Sb powder with a purity of 99.999% was placed in a K-cell for thermal deposition in the UHV chamber. Then Sb in the K-cell was degassed in the chamber prior to the silicon substrate preparation above.

K-cell was heated up to *ca.* 300 ºC, which increased the pressure in the chamber to 4.4×10^{-8} mbar, facing the Sb deposition beam towards the quartz microbalance to confirm the thermal deposition rate stability, which in this case was stabilized at 11.9 Hz/min $\pm$0.4%. The clean vicinal silicon substrate was then heated to 500 ºC prior to the Sb deposition. Then the sample is exposed to the Sb beam for 60 sec, in order to deposit Sb layers on the silicon surface. The sample was post-annealed at 500 ºC for 30 min, with

the intention to desorb excess layers of Sb above the monolayer coverage. [52] After this procedure, the chamber pressure recovered 2.1 × 10^{-10} mbar. Then, low electron energy diffraction (LEED) and UHV-STM were performed on the Sb-passivated vicinal Si(111) surface.

4.2.3 CuPc deposition

CuPc (sublimed grade (>98.5%), purchased from SynTec GmbH, Germany) was then deposited on the sample after completing the observation by LEED and UHV-STM. Before CuPc deposition, the K-cell was heated to about 465 º C under 1.2 x 10^{-10} mbar, which stabilized the molecular beam deposition rate at 2.4 Hz/min ±2% on the quartz microbalance, which shall deposit the molecular layer at the rate of 0.3 ML/min. Then the sample at room temperature was exposed to a molecular beam for 60 sec. The deposition conditions are optimized so it can form a single molecular layer on the surface with less than full coverage. It is also to be noted that the absolute deposition rate of CuPc may vary depending on the experimental setup. Then the sample was post-annealed at 150 °C for 2 min. In order to avoid the thermal drift effect under UHV-STM over a relatively larger scan area, the low-temperature STM (LT-STM) was performed at -233 °C.

4.3 CuPc topography on Sb passivated stepped Si surface

Fig. 4.2 displays the vicinal silicon surface with Sb deposition passivation on Si(111)-7x7 reconstruction. As expected from the previous chapters in this Study, the vicinal silicon surface exerted the long-range steps and terraces, preserved after the Sb passivation process. The terrace width in this image varies from *ca.*2 to 6 x 10 nm.

Fig. 4.3 shows (a) the topographic image with constant current mode image and (b) its z-displacement normalized image with plane subtraction of the same scan area. The steps and the terraces are observed clearly over a substantial span of the surface.

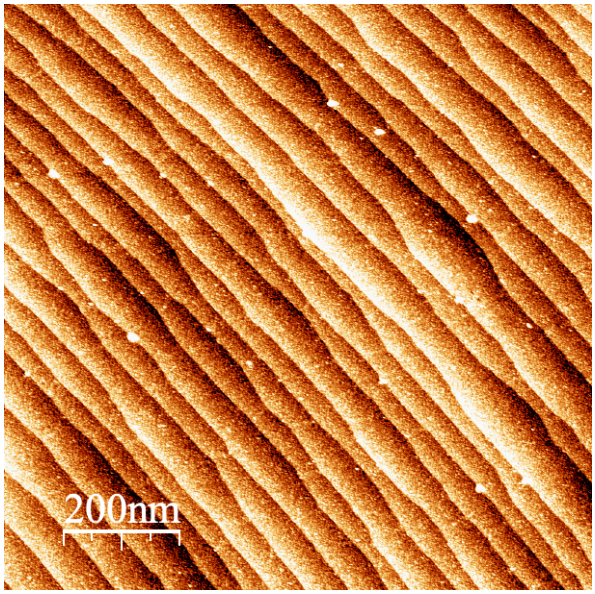

Fig. 4.2 Sb passivated 0.35º vicinal Si(111) surface observed by LT UHV-STM with constant current mode at 0.4nA, +1.0 sample bias voltage. Steps and terraces are confirmed on large surface area, extended to sub-micrometer range.

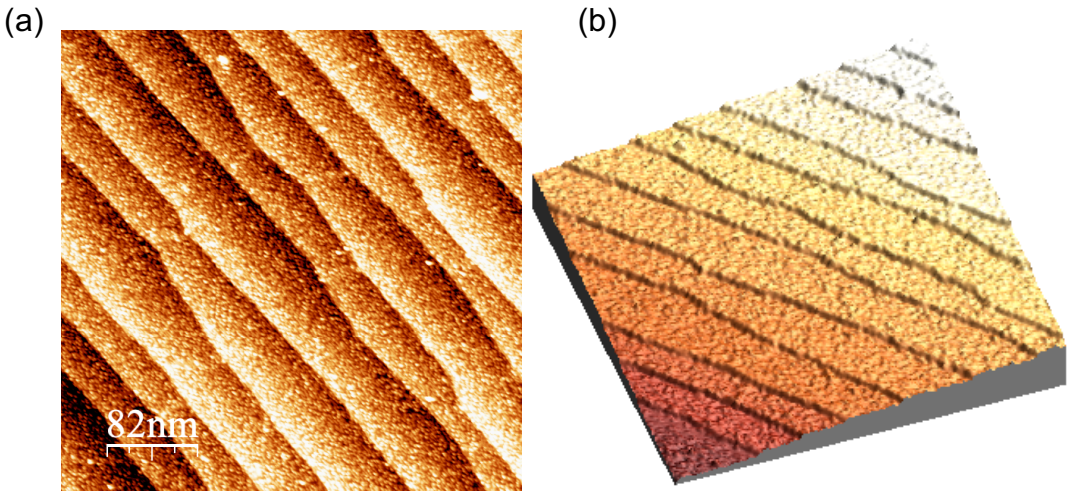

Fig. 4.3 Detailed STM image on the vicinal Sb-Si(111) surface with LT-UHV-STM. (a) Contrast image (0.4nA, +0.1V) (b) its 3D plot.

It is also important to observe the smoothness of the step edges in order for the subsequent study with low dimensional structure formation with organic molecules induced by the step edges.

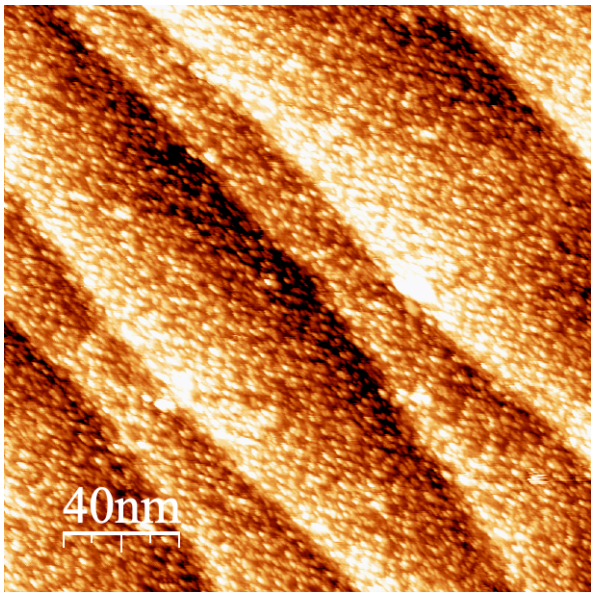

Fig. 4.4 Sb passivated 0.35º vicinal Si(111) surface observed by LT UHV-STM with constant current mode at 0.4nA, +1.0 sample bias voltage. Steps and terraces are confirmed on large surface area, extended to sub-micrometer range

Fig. 4.4 shows the typical topography around the step edges after Sb deposition. It confirms that there is no significant accumulation of excess Sb atoms on the step edges. As a result, the step and terrace feature of the underneath vicinal Si(111) substrate is maintained as intended by this Study.

Furthermore, Fig. 4.5 confirms the typical height profile of a single step after Sb deposition. From the direct observation of the step height, it is confirmed that the

single step is keeping the bilayer height profile of the vicinal silicon surface underneath, which indicates the Sb layer is monatomic.

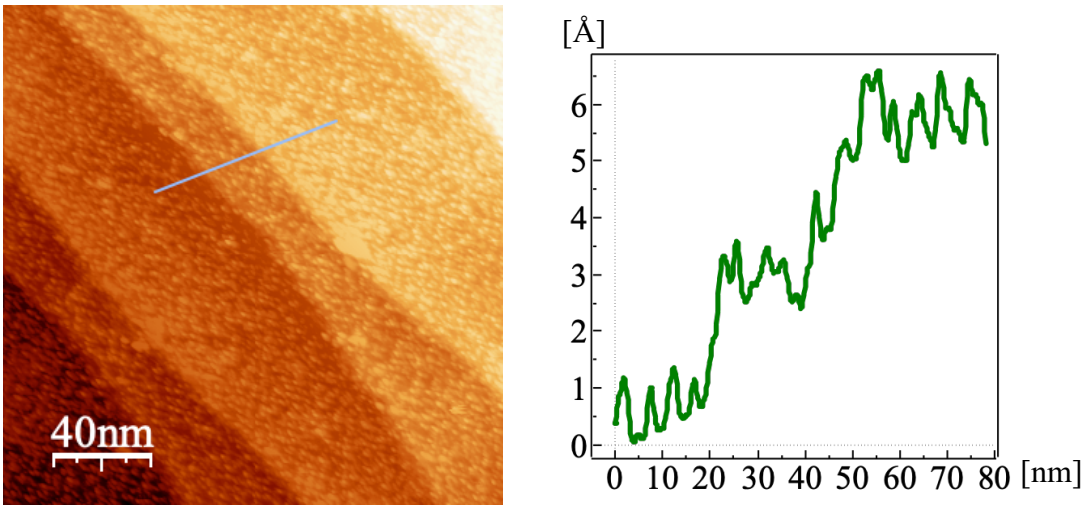

Fig. 4.5 Base line normalized topography of the vicinal Sb-Si(111) stepped surface and the height profile of a typical steps and terraces.

Fig. 4.6 shows closer observation on (a) a plateau of a terrace and (b) across a step edge. The smooth surface after Sb passivation is also confirmed by the roughness of the scanned area. The RMS roughness of the terrace and across the step edge is; 0.068 nm and 0.083 nm, respectively. The higher RMS roughness on the latter image is due to the nature of the step height in the scanning area.

In Fig. 4.6 (a), the bright spots indicated by circles are typical Sb clusters, whereas the darker feature indicated by squares are considered to be Sb layers on Si(111) surface. [71, 72, 73]

(a) (b)

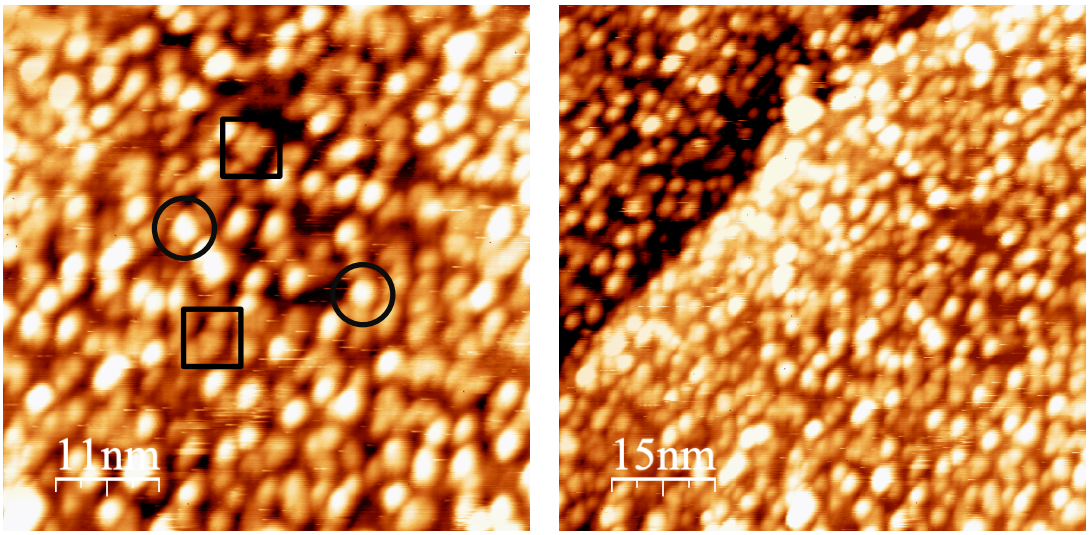

Fig. 4.6 (a) constant current image on the plateau of a terrace and (b) scan area including a step edge. (constant current mode, 0.3 nA, 2.5 V) RMS roughness: 0.068 nm and 0.083 nm respectively. The RMS roughness confirms the atomic smoothness of the surface after passivation. The RMS roughness on (b) is greater than (a) due to the nature of step edge height variation. The bright spots of which typical feature are indicated by circles in (a) are Sb clusters, whereas the darker feature indicated by squares are considered to be Sb layers on Si(111) surface. [72, 73]

The bright spots with a diameter of *ca.* 3 nm indicated in the green circle in Fig. 4.7 (a) and inset A, are considered Sb clusters. In the analysis of Fig. 4.6, the STM image on Sb/Si(111) surface is compared to the previous reports from others on the surface prepared in a similar manner. In Fig. 4.7 are the cited images from the previous reports. The images are scaled to fit the same magnification as our image.

Inset B shows a comprehensive local structure of Sb adatom and underlying layers of Sb and Si. The blur feature in Fig. 4.7 (a) marked with a red circle, resembles the Sb adatom and second over-layer Sb atom in the report by *K.H. Park et al.* [74]

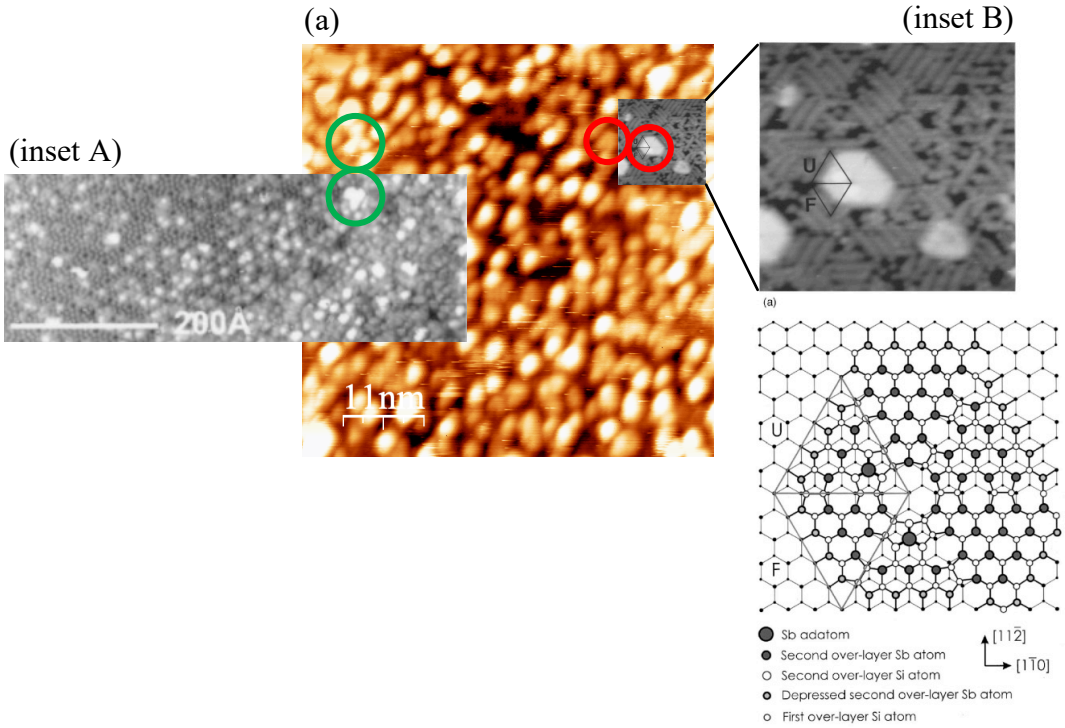

Fig. 4.7 (a) the same data from Fig. 4.6 (a) for comparison. (Inset A) *Voigtländer et al.* [71] Fig.4 therein.[1] (Inset B) *Kang-Ho Park et al* [74]. Fig. 2 therein.[2] Both insets are scaled to the same magnification of (a). The bright spots indicated by circles are typical Sb clusters, whereas the darker feature indicated by squares are considered to be Sb layers on Si(111) surface. Inset B shows a comprehensive local structure of Sb adatom and underlying layers of Sb and Si. The blur feature in Fig. 4.7 (a) marked with a red circle, resembles the Sb adatom and second over-layer Sb atom in the report by *K.H. Park et al*.

Although it is difficult to show the Sb surface structure from our image only, the comprehensive comparisons with the previous reports conclude that the bright spots in our image are Sb clusters, which lay on the underlying Sb-Si structure. The

[1] Reprinted from Surface Science, vol. 464, 2000, B. Voigtländer and M. Kästner, "Measurement of Sb diffusion using shadow profiles created by a STM tip," pp. 131-144, Copyright (2021), with permission from Elsevier.

[2] Reprinted with permission from Journal of Vacuum Science & Technology A, vol. 15, 1997, K.-H. Park, J. S. Ha, W. S. Yun, E.-H. Lee, J.-Y. Yi and S.-J. Park, "Scanning tunneling microscope study of Sb / Si(111)-√3x5√3 structure," p.1572, Copyright (2021), American Vacuum Society.

density of the Sb cluster is measured to be 7.5 x 10^{-2} nm^{-2}, for 226 Sb clusters observed in this scanned area of 55 x 55 nm^2. The average size of the cluster is 2.8 nm^2, and the typical diameter ranges between 2-4 nm, which are elongated more often than not. A detailed study on a similar surface condition is reported elsewhere. [53, 75, 76, 77, 71, 72, 74]

Fig. 4.8 shows the LEED pattern comparison of the bare vicinal silicon surface after 7x7 reconstruction procedure (a), and after Sb passivation (b). These LEED studies were performed on the identical sample, which was studied by UHV-STM discussed above. The LEED pattern confirms the signature of 7x7 reconstruction on the bare silicon surface before Sb passivation. After the Sb passivation, it is confirmed that the three-fold symmetry from the Si substrate is preserved. By comparing with the earlier report [76], this sample exerts the indication of √3 x √3 surface reconstruction and epitaxial growth of the Sb layer from the prominent diffraction pattern. The √3 x √3 surface reconstruction and

(a) (b)

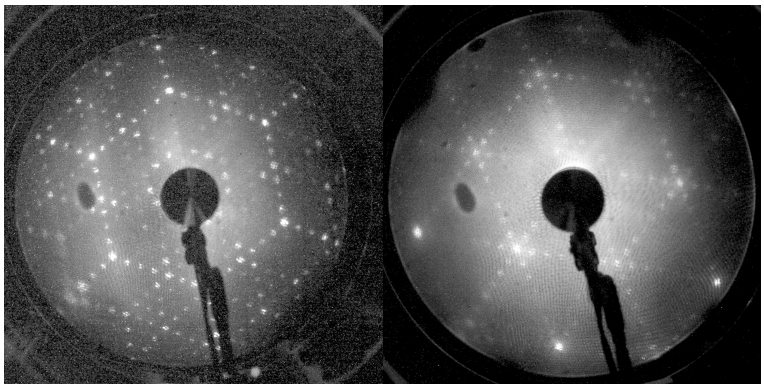

Fig. 4.8 LEED pattern (a) clean Si(111)-7x7 reconstructed vicinal surface. Electron beam energy at 60.1 eV (b) Sb-Si(111) surface with bean energy at 73.5 eV. The superstructure of the surface reconstruction can be observed even after Sb passivation.

from the temperature of the sample surface during the deposition and desorption of Sb, *i.e., ca.* 500 ºC. The thickness of the Sb layer is estimated to be *ca.* 1 ML according to the phase diagram of the earlier reports. [53, 76]

Fig. 4.9 displays the UHV-STM image on the sub-monolayer of CuPc deposited on the prepared substrate above. The Sb passivated surface (dark) and CuPc domains (white) can be seen at the same time, which confirms the sub-monolayer deposition.

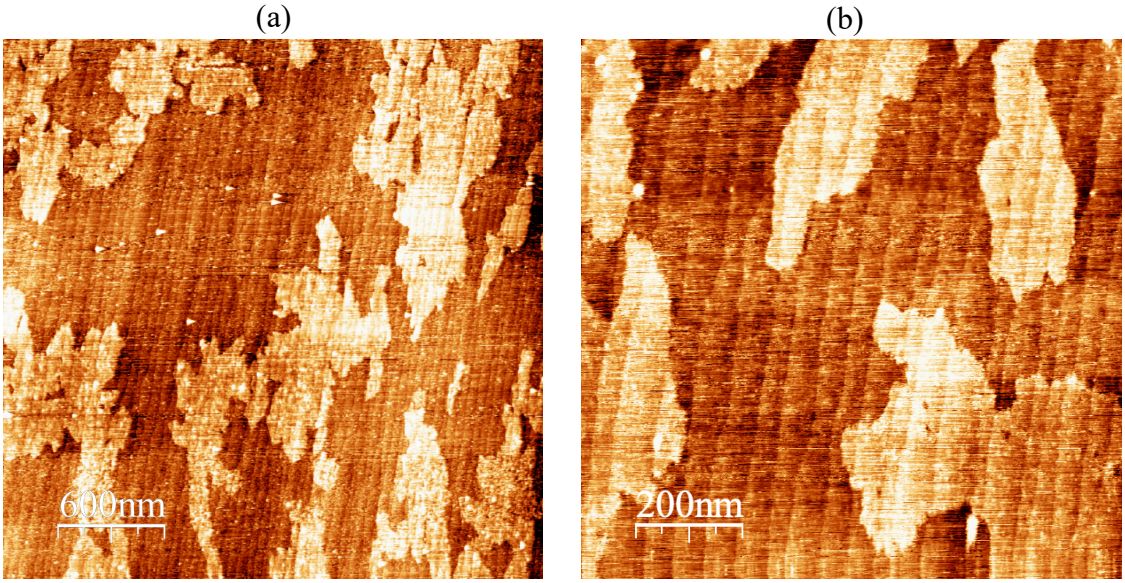

Fig. 4.9 LT-UHV-STM topography image on CuPc submonolayer on the Sb passivated vicinal silicon surface. Long strips elongated vertically are the steps of the vicinal surface. Island growth of CuPc submonolayer is observed. CuPc islands tend to cover the terraces more than across the step edges. (a) 3000 x 3000 nm^2 (b) 1000 x 1000 nm^2. (constant current mode, 0.3 nA, 2.5 V)

Firstly, the growth of large domains of CuPc is observed over the sub-micrometer range. Despite the sparse CuPc deposition, CuPc sub-monolayer resulted in the formation of densely packed islands well separated from each other. The separation of CuPc islands can be more than 150 nm apart. Secondly, each CuPc domain tends to elongate parallel to

the step edges. The islands of CuPc first deplete the terraces, than crossing over the step edges to occupy neighboring terraces. Thirdly, it is also worth noticing that there is no accumulation of CuPc on the step edges on the surface outside the islands.

Since CuPc is randomly landing on the surface by the molecular beam deposition, the formation of the island domains is demonstrating the substantial mobility of CuPc on this surface.

[Molecular-Substrate configuration]

There are two different molecule-substrate configurations with different binding energies, as depicted in Fig. 4.10: Configuration (α) molecular plane parallel to the substrate surface and Configuration (β) molecular plane perpendicular to the substrate surface where Configuration (α) is usually considered more stable than Configuration (β).

[Molecular-Molecular configuration]

There are two molecule-molecule configurations at the substrate surface: two neighboring molecules with their planes parallel to the substrate surface as expected in Configuration (α), and two molecules with their planes perpendicular to the substrate surface as expected in Configuration (β), where the latter enables a rather strong molecule-molecule interaction due to the columnar stacking which may easily overcompensate the lower molecule-substrate binding.

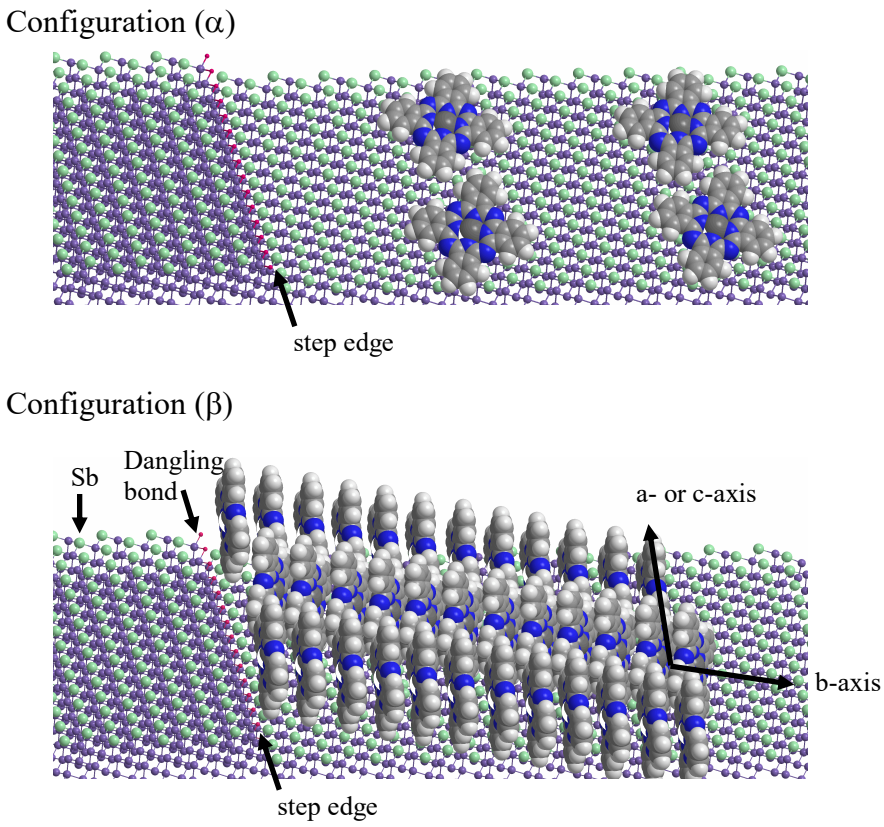

Fig. 4.10 The discussed models of the stacking of CuPc orientation with respect to the substrate. Configuration (α) shows CuPc molecular plane parallel to substrate surface, whereas Configuration (β) shows molecular plane perpendicular to substrate surface. The substrate in the model depicts only stepped silicon surface beneath Sb passivated layer, in order to make emphasis on the relative configuration of CuPc and the surface. Identified with red is the step edge.

Namely, CuPc can overcome the local binding force on Sb-passivated Si(111) surface and can move to the extent to find the neighboring island domain. At the same time, the intermolecular attraction force between CuPc is strong enough to pin the molecule to the island that it is attaching to. This is evident from the fact that CuPc self-aggregated on the Sb passivated surface.

It could fairly well be that during preparation, the molecules are mainly landing with their planes parallel to the surface and diffuse this way at low coverage over the substrate surface. With increasing coverage, molecule-molecule interactions come into play where the erection of the mass of the diffusing molecules be eased when they cross a step edge on the substrate.

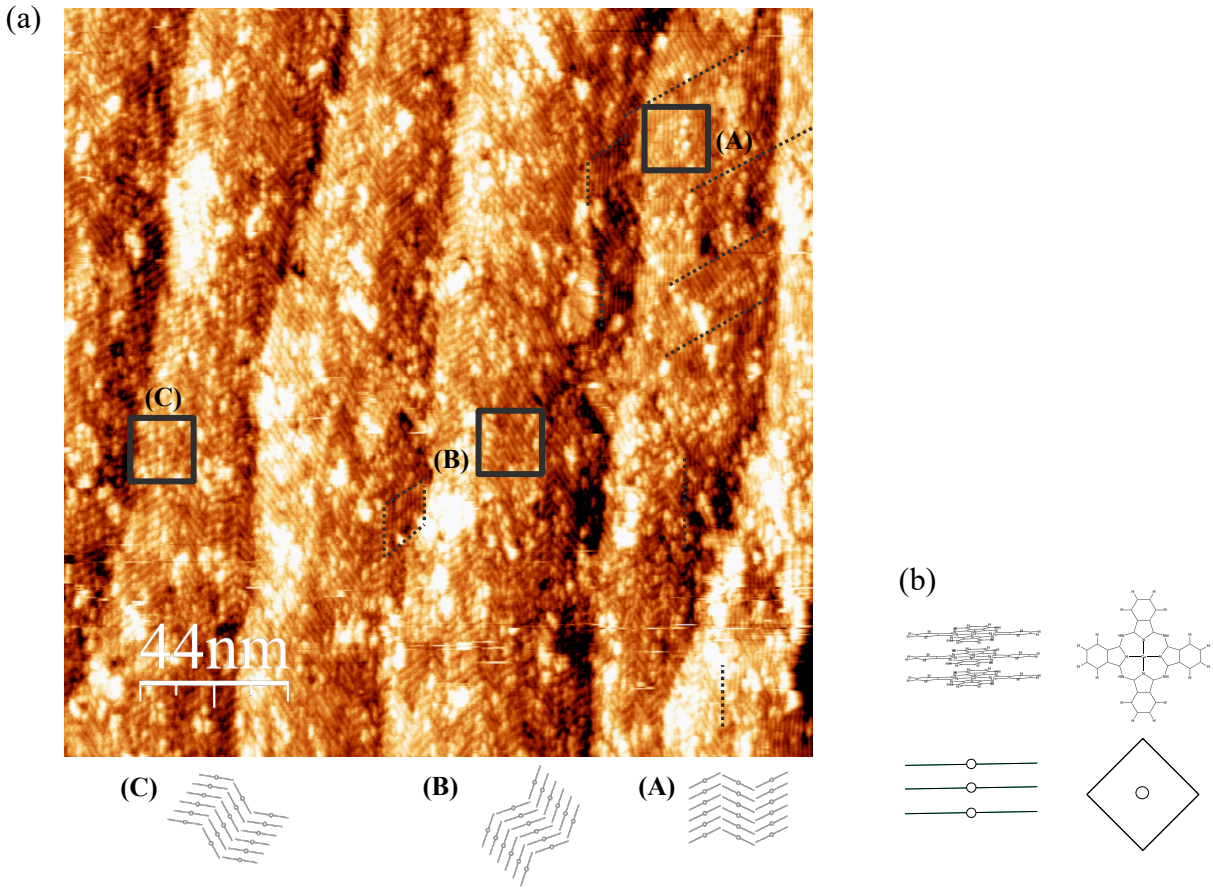

Fig 4.11 (a) Detailed STM image on a CuPc island. The fine stripe-like feature confirms columnar growth mode of CuPc parallel to the surface. Marked by squares are the typical orientation of columns in each domain where the features are mor prominent. CuPc molecule's in-plane direction is parallel to the step edges dominantly. The same characteristics are confirmed on other islands of CuPc sub-monolayer too. (constant current mode, 0.3 nA, 2.5 V) (b) schematic drawing of the CuPc profile.

It is also derived that the attraction force of CuPc to form the island on the terrace (CuPc-Terrace) is stronger than CuPc attaching to the step edges (CuPc-Step) because if CuPc is attaching to the step edges stronger than the attraction force to form island domain, CuPc should have first aggregated along the step edges before forming the island. However, the finding of this report does not show aggregation of CuPc along the step edges before the island formation, which contradicts the finding of this Study.

Fig 4.11 shows the detailed topography of a CuPc island on an identical surface. CuPc clearly exerts organized structures. There are columnar structures, expanding in 3 different directions, which create domains. The typical columnar features are identified by squares in Fig 4.11 as (A), (B), and (C) in the middle of each domain. The distance between the columns is statistically measured, which are 1.5 ± 0.1 nm, 1.8 ± 0.2 nm, and 2.4 ± 0.3 nm for Domain A, B, and C, respectably. These distances are in alignment with the previous reports, which are compared in Table 4-1. This confirms that the columnar feature in Fig 4.11 is CuPc columns lying on the surface. [16, 78]

Table 4-1 Previously reported distances between columns of CuPc in crystalline structures. a- and c-axis refer the crystallographic orientation as depicted in Fig. 3.5.

a-axis [nm]	**c-axis [nm]**	**Reported by**
1.50	1.57	*Nakamura et al.* [16]
1.20	1.30	*Hiesgen et al.* [78]

Fig. 4.12 illustrates the distinct domains of columnar growth modes, carefully observed at the step edge with a kink of the step edge. CuPc is well aligned along the step

edges by stacking each other, as depicted in the Configuration (β) in Fig. 4.10. The columns of CuPc stack are lying flat on the surface.

It is also observed that the majority of CuPc' in-plane direction is diagonal to the step edges, in this case $[11\bar{2}]$ direction. Namely, Domain B and C in Fig 4.11 are more dominant over Domain A. In fact, Domain A covers only 14% of the surface on this sample, whereas Domain B, C collectively covers 86%, which shows the anisotropy of the columnar growth mode.

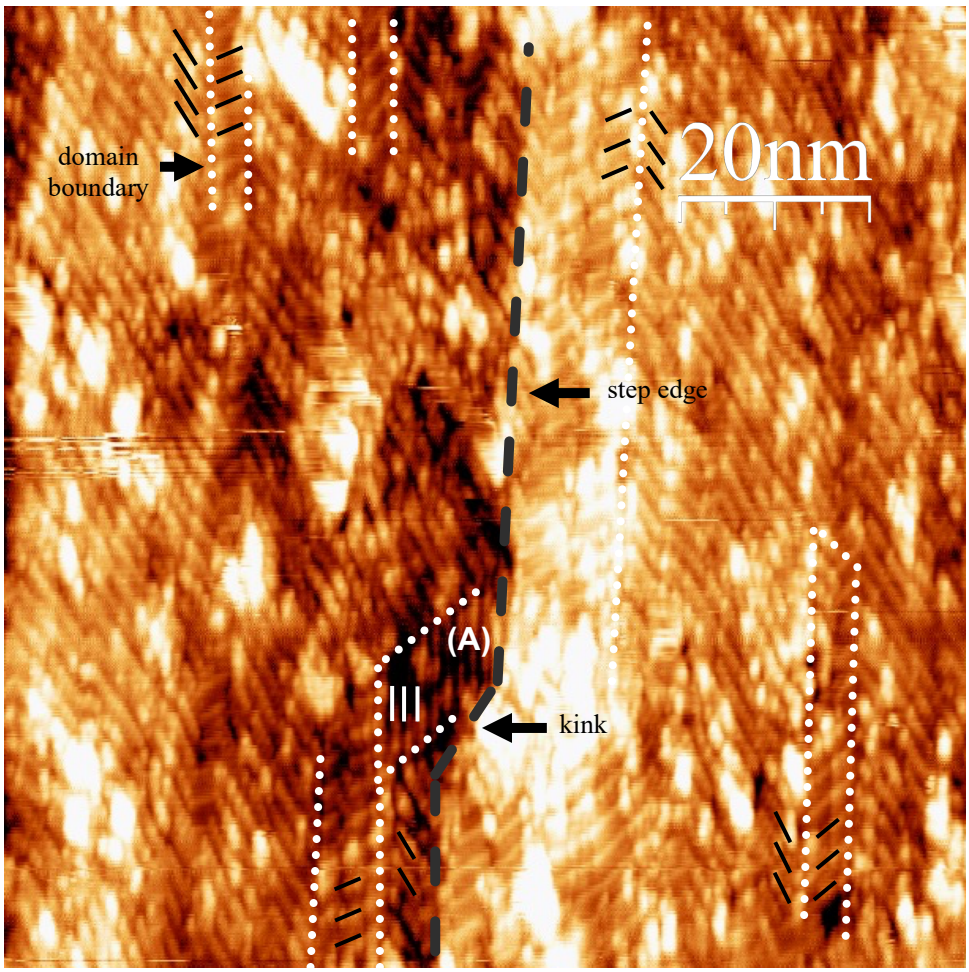

Fig. 4.12 Columns of CuPc along the step edge around a kink, and identified domains of the columnar growth modes. Several domains are observed adjacent to each other. Anomaly of columnar direction is observed around the kink of the step edge. (constant current mode, 0.3 nA, 2.5 V)

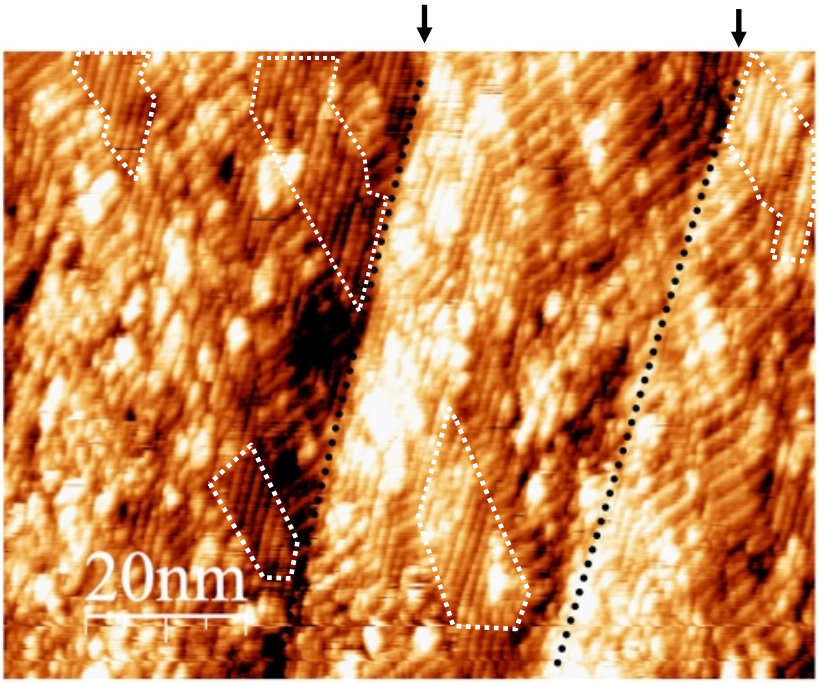

Fig. 4.13 Anomaly of the growth mode on the terrace between unparalleled step edges. The majority of the columns are parallel to the step edge, although both growth modes were found. (constant current mode, 0.3 nA, 2.5 V)

While the majority of CuPc orientation is diagonal to the step edges, *i.e.,* Domain B or C, it could observe some domains perpendicular to the step edges, especially around the kinks of the step edges, *i.e.,* Domain A. Fig. 4.13 is an example of Domain A. It is interesting to note that such columnar growth tends to be found around the kinks of step edges (indicated as (A) in Fig. 4.12), or the step edges that are not parallel to adjacent step edge, where prominent features are marked in dashed white line in Fig. 4.13. Though the majority of CuPc in-plane direction is diagonal to the step edges, certain parts on the island showed an anomaly in the orientation.

4.4 Summary

It is confirmed that Sb passivated stepped vicinal Si(111)-7x7 surface can induce the ordered growth mode of CuPc sub-monolayer, with CuPc in-plane direction diagonal to the step edges.

Surprisingly, the orientation of the CuPc columns is diagonal to the step edges of the vicinal surface, contrary to the findings on the H passivated surface. Sb passivated Si(111) surface allows substantial molecular diffusion of CuPc, which is confirmed by the island growth. At the same time, it is confirmed that CuPc-CuPc intermolecular interaction is stronger than CuPc-Step attraction force, only in which case CuPc can exert the island growth before aggregation to the step edges. It is also shown that there is anisotropy in the columnar growth direction.

The successful control of CuPc thin film order by Sb passivation versus H passivation gives insights on the practical processing of such a hybrid device utilizing the Sb passivation, which is more practical than H passivation in terms of process accessibility.

5 Analysis and comparison with the recent studies

From these observations, CuPc on the passivated stepped surface is confirmed to exert a self-assembly feature. On H passivated vicinal Si(111) surface, CuPc formed columns that are parallel to the step edges in the middle of the terrace. On Sb passivated vicinal Si(111) surface, the CuPc grows columns of which the majority aligned diagonally to the step edges. Such columnar growth is confirmed to extend on the terraces, on the area isolated from the step edges apart for more than 100 nm order.

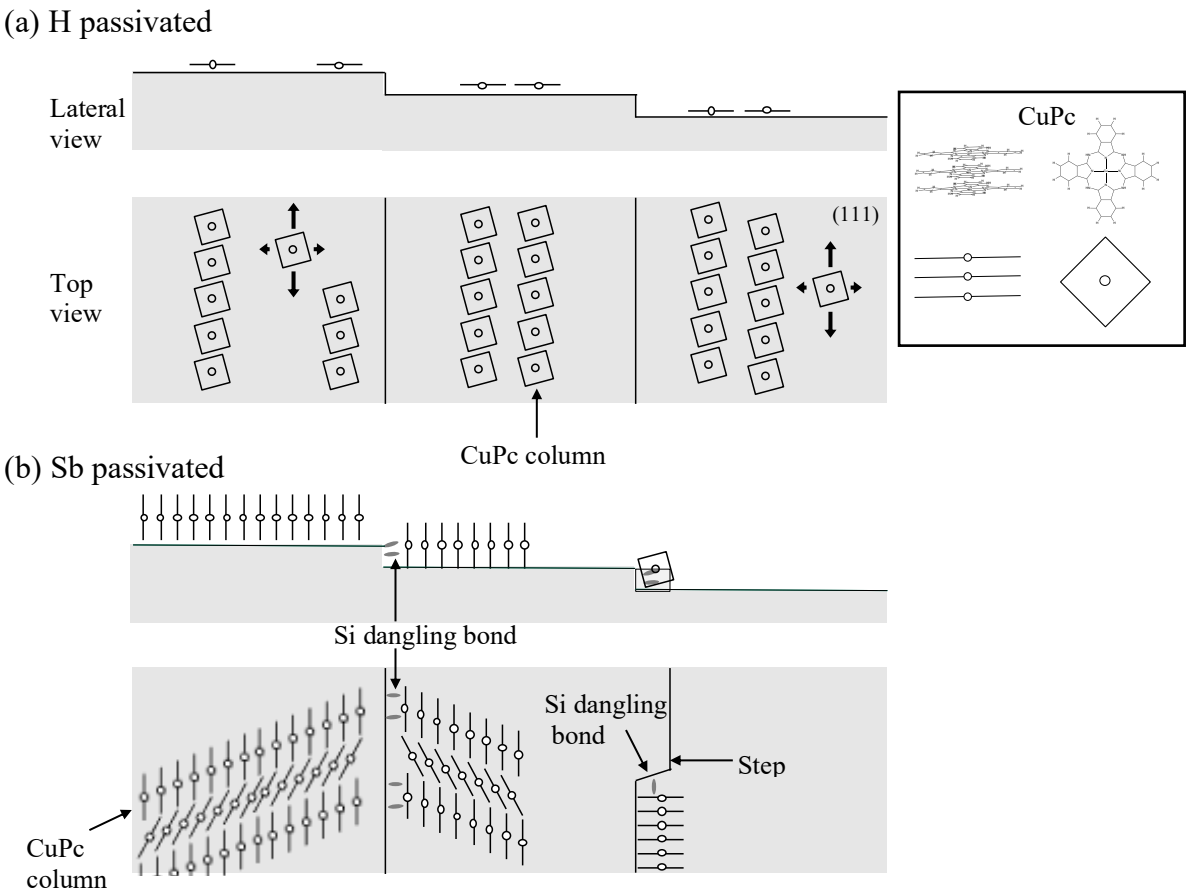

Fig. 5.1 Proposed model of CuPc self-assembled alignment on (a) H passivated and (b) Sb passivated vicinal Si(111) substrates.

From the images in the same magnifications, it is more obvious that the configuration of CuPc is different between H and Sb passivated surfaces with respect to the surface. Fig. 5.1 shows the summary of the findings of this Study and the corresponding models of CuPc and vicinal Si stepped substrate.

On Sb passivated vicinal silicon surface, the dangling bonds on a terrace are all deactivated by Sb termination, while the step edge leaves the dangling bonds unterminated. CuPc on the terrace is mobile enough on the deactivated Sb-Si(111) surface until it reaches the dangling bond on the step edge to be pinned. The in-plane direction of CuPc is attached perpendicular to the dangling bond. The CuPc which is attached to the step edge, serves as the nucleation site of the subsequent columnar growth. From the crystallographic nature of CuPc, the columns grow diagonal to the step edge.

On the contrary, on H passivated vicinal silicon surface, there is no dangling bond to pin CuPc. Thus, CuPc attaches to the substrate with more area of interaction, which is achieved by lying flat on the surface. The following observations support this conclusion.

5.1 The direction of one-dimensional growth of CuPc with respect to step edges

The surprising findings of CuPc column direction difference with respect to the step edge between H and Sb passivation can be explained by the surface passivation and the dangling bonds on the step edges.

[CuPc on clean Si(111)-7x7 surface]

On the clean Si(111)-7x7 substrate, CuPc is pinned at random sites on the terrace and shows no self-assembly feature, as shown in Fig. 3.10. This confirms that the dangling bonds on the Si(111)-7x7 is acting as the anchor to CuPc, which explains the random sites of CuPc attachment. Noticeably, CuPc is lying flat on the substrate depicted as Configuration (α) in Fig. 4.10. It is concluded that the CuPc in-plane orientation is perpendicular to the direction of the dangling bonds, which in this case are sticking out perpendicular from Si(111)-7x7surface.

[CuPc on H-Si(111) surface]

On H-passivated Si(111) surface, the atomic hydrogen terminates the dangling bonds on the surface, including the terraces and the step edges, to which leaves no anchor to CuPc to attach. As confirmed in the thermal desorption experiment in Fig. 3.9, CuPc is weakly interacting with H-passivated Si(111) surface, which allows CuPc to lie flat, which coincides with earlier reports.[16, 28] CuPc is laterally mobile on this condition on a terrace, which may have been bounced back and forth between two step edges.

The molecular mobility on the steps and terraces on a crystalline surface are discussed and studied in the light of the surface potential barrier, which was originally reported theoretically by *Schwoebel et al.* [68] and experimentally by *Ehrlich et al.* [79]. The reports discussed the mechanism of the growth of the mobile atom on the top surface, where it encounters a potential barrier at the step edge, referred to as the Ehrlich-Schwoebel barrier (ESB). (Fig. 5.2) The ESB barrier gives rise to the potential barrier at the step edge, where not only an atom but also organic molecules going over the step towards descending direction may also experience the potential barrier and can be bounced back to the terrace. [69]

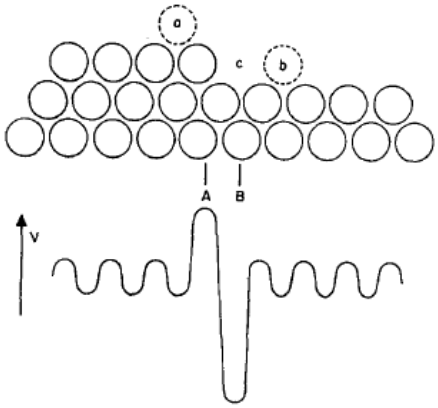

Fig. 5.2 Potential diagram over the step edge proposed by *Schwoebel et al.* [68] The cross section of a monatomic step in a surface is schematically represented. The step edge between A and B gives rise to the potential variation. Reproduced from *Schwoebel et al.* [68], with the permission of AIP Publishing.

Though H passivated Si(111) surface has three-fold symmetry in rotation, CuPc showed one-dimensional growth, which has lower rotational symmetry. The ESB potential by the step edges on H passivated Si(111) may explain the breaking of the symmetry of the rotation, which gives rise to the one-dimensional growth with the nucleation sites even in the middle of terraces.

[CuPc on Sb-Si(111) surface]

On Sb-passivated Si(111) surface, contrary to the H-passivated surface, the step edges play an important role in the nucleation of the columnar growth of CuPc. The phenomena can be explained by the excess dangling bonds on the step edges, whereas the dangling bonds on the terrace are terminated by Sb passivation.

The dangling bonds on Si(111) surface can be terminated by Sb on a flat surface, as previously reported, as depicted in Fig. 5.3. [80] However, such termination may not be expected on the side of the step edges or the step kinks, where the crystal structures are altered. Thus, it is plausible to assume the dangling bonds still remain active on the side of the step edge and the step kinks.

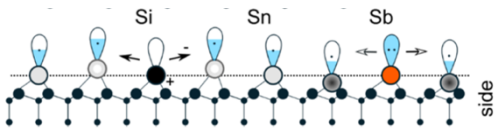

Fig. 5.3 *Zimmermann et al.* [80] reported the Sb atom terminates the Si(111) surface by substitution, leaving no unpaired dangling bonds. [3]

From the finding from CuPc on a clean Si(111)-7x7, it is anticipated that CuPc in-plane orientation attaches perpendicular to the dangling bonds. Since CuPc is mobile on the substrate when landing randomly on the terrace, CuPc moves around until it is pinned by the dangling bond on the step edges or kinks, as illustrated in Fig. 5.1. Since

[3] Reprinted (adapted) with permission from J. Phys. Chem., vol. 123, 2019, P. Zimmermann, K. Majer, P. Kocan, I. Ostadal and P. Sobotik, "Role of Dangling Bond State Occupancy in Adsorpotion of Copper Phthalocyanine on Si(111)-Sn- √3x√3," pp. 16232-16238, Copyright (2021) American Chemical Society.

CuPc is pinned perpendicular to the dangling bond, CuPc stands perpendicular to the surface as Configuration (β) in Fig. 4.10. After the first CuPc attached to the step edge or kink, this CuPc serves as the nucleation site for the subsequent CuPc columnar growth. Due to the crystallographic stability, CuPc columns grow diagonal to the step edges which can be understood from the CuPc bulk structure reported elsewhere. [16, 28, 29, 78] By this mechanism, the domain (A), (B) in Fig 4.11 can be understood. As to domain (A), the straight columnar growth can be the result of the anchor effect due to the dangling bonds both on kinks and the step edges.

Wagner et al. [77] reported the growth mode of zinc phthalocyanine thin film on the deactivated Si(111) surface with steps and terraces. In their study showed the zinc phthalocyanine grew columnar structure perpendicular to the step edges, which shows a similar trend to the findings of this Study. (Fig. 5.4) Both results can be understood from the attachment of CuPc to the dangling bonds on the step edges.

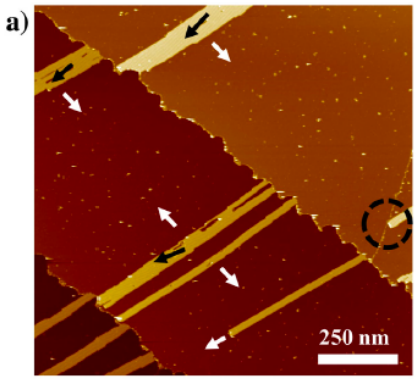

Fig. 5.4 STM topography of sub-monolayer zinc phthalocyanine molecules on Si(111)-B √3 x √3R30° surface. [77] The columns of Pc molecules grow perpendicular to the step edge.[4]

[4] Reprinted from Surface Science, Vols. 22- 27, no. 630, 2014, S. R. Wagner and P. Zhang, "Nucleation and evolution of zinc phthalocyanine thin films on the deactivated Si(111)-B√3 x √3 R30° surface," Copyright (2021), with permission from Elsevier.

Similar attempts to control the molecular superstructure utilizing the silicon stepped surface was reported by *Nakamura et al.* [28] In their study, phthalocyanine thin film was formed on the H passivated Si(001)-2x1 reconstructed surface. (Fig. 5.5) Their results show the bidirectional growth of CuPc on the H passivated Si(001)-2x1 surface with the step separation of *ca.* 4 nm. CuPc thin film topographies confirm bidirectional but non-selective growth mode with respect to the step edges. The square-like growth mode on Si(001) may be attributed to the rotational symmetry of the Si(001)-2x1surface structure when collectively understood with the report, whereas on Si(111) surface showed three-fold symmetry in rotation of CuPc thin film. [29] Namely, CuPc thin film structure inherits the rotational symmetry of the Si substrate. However, these results cannot be directly compared due to the large difference in the average step widths, *i.e.,* 4 nm (*Nakamura et al.*) and 90 nm (this Study).

(a)

(b)

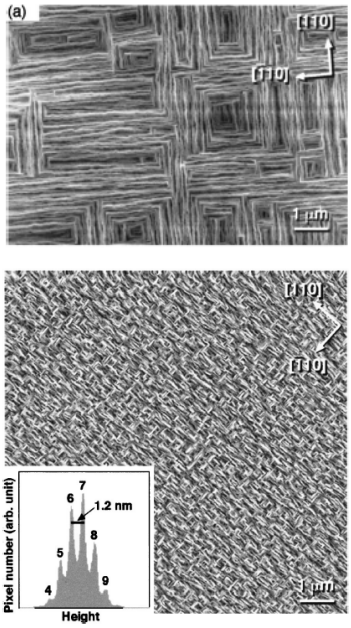

Fig. 5.5 (a)AFM topography of CuPc film deposited on flat Si(001)-2x1-H surface at 60 °C. Bidirectional molecular stack formation can be observed. (b) AFM image of CuPc deposited on vicinal Si(001)-2x1-H surface with *ca.* 4 nm regular step separation. Reproduced from *Nakamura et al.* [28], with the permission of AIP Publishing.

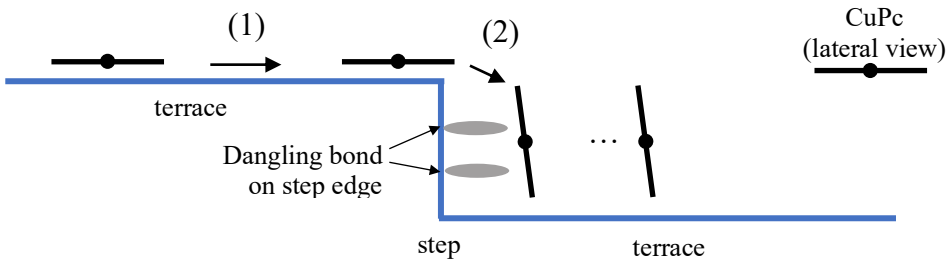

Fig. 5.6 Schematic model of dynamic behavior of CuPc. (1) As CuPc molecule laterally moves over surface over step edge, or roughness in general, (2) such surface alternation may contribute to induce "flipping" of CuPc by disturbing the area of contact between CuPc and the substrate, which will help CuPc pinned to the dangling bond on the step edge. Such dynamics need to be understood not in the conventional mechanics with gravity, but rather in the quantum mechanical forces. (reproduced from the private discussion with Prof. Dr. M. Hietschold, Chemnitz University of Technology, Germany, and with Prof. Dr. Y. Takakuwa, Tohoku University, Japan)

The molecular mobility across the step edge may also encourage the nucleation of CuPc on the dangling bonds at the step edge. One of the possible explanations for such behavior of CuPc can be explained in the model, as depicted in Fig. 5.6. As CuPc molecule laterally moves on the surface over a step edge, such surface alternation may contribute to induce "flipping" of CuPc by disturbing the area of contact between CuPc and the substrate, which eventually helps CuPc to attach to the dangling bonds on the step edge. Such dynamics need to be understood not in the conventional mechanics with gravity but rather in the quantum mechanical forces.

6 Conclusion

As anticipated in the purpose of the Study, the alignment of CuPc can be substantially controlled by the dangling bonds on the step edges acting as an anchor, whereas on the terraces, the molecular mobility is maintained to allow CuPc to self-assemble the superstructure.

It is confirmed that the step structure of the vicinal silicon surface determines the growth mode of CuPc thin film, inducing anisotropy of CuPc orientation. The detailed orientation of CuPc in the thin film showed a surprising effect by surface passivation either with H or Sb.

Both H passivation and Sb passivation on Si(111) surface induce substantial molecular mobility of CuPc on the terraces, which resulted in long-range island growth due to the dangling bonds terminated by the surface passivation. The island growth confirmed that CuPc-CuPc intermolecular interaction is stronger than the CuPc-Step attraction force, only in which case CuPc can form such islands.

To the surprise, sparsely deposited CuPc exerted a one-dimensional structure parallel to the step edges in the middle of a wide terrace on the vicinal H passivated

Si(111)-7x7 surface. The effect of the step edge direction is evident. The Ehrlich-Schwoebel barrier is proposed as a speculated mechanism that induces such one-dimensional alignment with the step edges of the Si substrate.

On Sb passivated Si(111)-7x7 surface, the orientation of the CuPc columns is diagonal to the step edges of the vicinal surface, contrary to the findings on the H passivated surface, which is anticipated due to the dangling bonds on the step edges and on the step kinks. Sb passivated Si(111) surface allows substantial molecular diffusion of CuPc, which is confirmed by the island growth.

It is also found that CuPc in-plane orientation differs between H passivated and Sb passivated surface, where CuPc lays flat on the surface on H passivated Si(111)-7x7 surface, depicted as Configuration (α) in Fig. 4.10. On the contrary, CuPc stands vertical on Sb passivated Si(111)-7x7 surface, depicted as Configuration (β). The vertical configuration of CuPc can be explained by two mechanism that is; (1) nucleation of CuPc on the dangling bonds on the side of the step edges on Sb passivated surface, and (2) the flipping effect on a relatively rough surface due to Sb clustering on Si(111) surface.

From the comparison of these studies, it is deduced that the low-dimensional molecular structure can be controlled by selecting the surface passivation, which gives rise to the molecular mobility, and the anchor effect due to the step edges on the vicinal silicon surface.

On Sb passivated vicinal silicon surface, the dangling bonds on a terrace are all deactivated by Sb termination, while the step edge leaves the dangling bonds unterminated. CuPc on the terrace is mobile enough on the deactivated Sb-Si(111) surface, until it reaches the dangling bond on the step edge to be pinned. The in-plane direction of CuPc is attached perpendicular to the dangling bond. The CuPc which is attached to the step edge, serves as the nucleation site of the subsequent columnar growth. From the crystallographic nature of CuPc, the columns grow diagonal to the step edge.

On H passivated vicinal silicon surface, there is no dangling bonds to pin CuPc. Thus, CuPc attaches to the substrate with more area of interaction, which is achieved by lying flat on the surface. The following observations support this conclusion.

The results of this Study indicate the fabrication of the low molecular superstructure on the silicon surface is accessible by optimizing these parameters, including vicinal silicon step density, surface passivation, and molecular mobility, possibly varying the deposition temperature.

Thanks to the recent advancement in surface technology, the silicon surface design technique is available for a wide variety of industrial applications. Further studies towards the realization of the organic-inorganic hybrid device are much anticipated utilizing the self-organizational feature of organic molecules when combined with the inorganic semiconductor surface with the foundation technologies.

7 Acknowledgment

The significant part of this Study was funded by Deutsche Forschungsgemeinschaft Graduiertenkolleg #829 “Akkumulation von einzelnen Molekülen zu Nanostrukturen.” The author would like to show his gratitude to Prof. Dr. Dietrich Zahn and Prof. Dr. Michael Hietschold of the Chemnitz University of Technology, for their insightful leadership and all the support that made it all possible. The author would like to thank the members of Sumitomo Corporation, and Dr. Takatoshi Yamada of National Institute of Advanced Industrial Science and Technology, and Prof. Dr. Ken Okano of International Christian University for their continuous and comprehensive support for the author over the years of pursuit of science.

8 Bibliography

[1] C. W. Tang, "Two-layer organic photovoltaic cell," *Applied Physics Letters,* vol. 48, p. 183, 1986.

[2] P. L. McEuen, "Single-wall carbon nanotubes," *Physics World,* Vols. 31-36, no. June, 2002.

[3] X. Duan, Y. Huang, Y. Cui, J. Wang and C. M. Lieber, "Indium phosphide nanowires as building blocks for nanoscale electronic and optoelectronic devices," *Nature,* vol. 409, no. 66-69, 2001.

[4] A. Hatzor and P. S. Weiss, "Molecular Rulers for Scaling Down Nanostructures," *Science,* vol. 291, no. 1019-1020, 2001.

[5] C. Kittel, Introduction to Solid State Physics, New York: John Wiley & Sons, Inc., 1974.

[6] J. Viernow, D. Y. Petrovykh, F. K. Men, A. Kirakosian, J. -L. Lin and F. J. Himpsel, "Linear arrays of CaF_2 nanostructures on Si, (and the reference therein)," *Applied Physics Letters,* vol. 74, no. 15, p. 2125, 1999.

[7] A. Kirakosian, J. -L. Lin, D. Y. Petrocykh, J. N. Crain and F. J. Himpsel, "Functionalization of silicon step arrays I: Au passivation of stepped Si(111) templates," *Journal of Applied Physics,* vol. 90, no. 7, pp. 3286-3290, 2001.

[8] D. M. Eigler, C. P. Lutz and W. E. Rudge, "An atomic switch realized with the scanning tunneling microscope," *Nature,* vol. 352, pp. 600-603, 1991.

[9] P. A. Sloan and R. E. Palmer, "Two-electron dissociation of single molecules by atomic manipulation at room temperature," *Nature,* vol. 434, pp. 367-371, 2005.

[10] D. M. Eigler and E. K. Schweizer, "Positioning single atoms with a scanning tunneling microscope," *Nature,* vol. 344, pp. 524-526, 1990.

[11] S. R. Forrest, "The path to ubiquitous and low-cost organic electronics," *Nature,* vol. 428, no. 911, 2004.

[12] S. F. Bent, "Organic functionalization of group IV semiconductor surfaces: principles, examples, applications, and prospects," *Surface Science,* vol. 500, no. 879-903, 2002.

[13] C. Joachim, J. K. Gimzewski and A. Aviram, "Electronics using hybrid-molecular and mono-molecular devices," *Nature,* vol. 408, pp. 541-548, 2000.

[14] T. A. Su, M. Neupane, M. L. Steigerwald, L. Venkataraman and C. Nuckolls, "Chemical principles of single-molecule electronics," *Nature Reviews Materials,* vol. 1, pp. 1-15, 2016.

[15] G. P. Lopinski, D. D. Wayner and R. A. Wolkow, "Self-directed growth of molecular nanostructures on silicon," *Nature,* vol. 406, pp. 48-51, 2000.

[16] M. Nakamura, Y. Morita, A. Ishitani and H. Tokumoto, " Molecular arrangement of copper phthalocyanine on hydrogen-terminated Si(111): Influence of surface roughness," *Journal of Vacuum Science & Technology,* vol. B 14, p. 1109, 1996.

[17] Y. Jiang and B. Tian, "Inorganic semiconductor biointerfaces," *Nature Review Materials,* vol. 3, pp. 473-490, 2018.

[18] J. Viernow, J. -L. Lin, D. Petrovykh, F. M. Leibsle, F. K. Men and F. J. Himpsel, "Regular step arrays on silicon," *Applied Physics,* vol. 72, no. 8, pp. 948-950, 1998.

[19] J. -L. Lin, D. Y. Petrovykh, J. Viernow, F. K. Men, D. J. Seo and F. J. Himpsel, "Formation of regular step arrays on Si(111) 7x7," *Journal of Applied Physics,* vol. 84, no. 1, pp. 255-260, 1998. https://doi.org/10.1063/1.368077

[20] A. Kirakosian, R. Bennewitz, J. N. Crain, T. Fauster, J. -L. Lin, D. Y. Petrovykh and F. J. Himpsel, "Atomically accurate Si grating with 5.73 nm period," *Applied Physics Letters,* vol. 79, no. 11, 2001.

[21] E. D. Williams and N. C. Bartelt, "Thermodynamics of Surface Morphology," *Science,* vol. 251, no. 4992, pp. 393-400, 1991.

[22] H. Rauscher, T. A. Jung, J. -L. Lin, A. Kirakosian, F. J. Himpsel, U. Rohr and K. Muellen, "One-dimensional confinement of organic molecules via selective adsorption on CaF_1 versus CaF_2," *Chemical Physics Letters,* vol. 303, pp. 363-367, 1999.

[23] T. Matsushima and C. Adachi, "Observation of Extremely High Current Densities on Order of MA/cm2 in Copper Phthalocyanine Thin-Film Devices with Submicron Active Areas," *Japanese Journal of Applied Physics,* vol. 46, no. 47, pp. 1179-1181, 2007.

[24] F. Yang, M. Shtein and S. R. Forrest, "Controlled growth of a molecular bulk heterojunction photovoltaic cell," *Nature Materials,* vol. 4, pp. 37-41, 2005.

[25] D. R. Zahn, N. G. Gavrila and M. Gorgoi, "The transport gap of organic semiconductors studied using the combination of direct and inverse photoemission," *Chemical Physics,* vol. 325, pp. 99-112, 2006.

[26] M. Hietschold, M. Toader, P. Schukrynau and L. Smykalla, "Ordered monolayers of metal phthalocyanines and rare-earth bisphthalocyanines on crystalline metal substrates - crystallographic and electronic structure," in *2011 11th IEEE International Conference on Nanotechnology*, Portland, OR, 2011.

[27] R. R. Lunt, J. B. Benziger and S. R. Forrest, "Growth of an Ordered Crystalline Organic Heterojunction," *Advanced Materials,* vol. 19, pp. 4229-4233, 2007.

[28] M. Nakamura, T. Matunobe and H. Tokumoto, "Control of in-plane orientation of phthalocyanine molecular columns," *Journal of Applied Physics,* vol. 89, no. 12, p. 10.1063/1.1373700, 2001. https://doi.org/10.1063/1.1373700

[29] M. Nakamura, Y. Morita and H. Tokumoto, "Influence of film thickness of the molecular arrangement of copper phthalocyanine on hydrogen-terminated Si(111)," *Applied Surface Science,* Vols. 113-114, pp. 316-321, 1997.

[30] L. Smykalla, C. Mende, M. Fronk, P. F. Siles, M. Hietschold, G. Salvan, D. R. Zahn, O. G. Schmidt, T. Rueffer and H. Lang, "(Metallo)porphyrins for potential materials science applications," *Journal of Nanotechnology,* vol. 8, pp. 1786-1800, 2017.

[31] L. Smykalla, P. Shukrynau, C. Mende, T. Rüffer, H. Lang and M. Hietschold, "Interplay of hydrogen bonding and molecule-substrate interaction in self-assembled

adlayer structures of a hydroxyphenyl-substituted porphyrin," *Surface Science,* vol. 628, pp. 132-140, 2014.

[32] M. Scheffler, L. Smykalla, D. Baumann, R. Schlegel, T. Hänke, M. Toader, B. Büchner, M. Hietschold and C. Hess, "Structual study of monolayer cobalt phthalocyanine adsorbed on graphite," *Surface Science,* vol. 608, pp. 55-60, 2013.

[33] M. Hietschold, M. Lackinger, S. Griessl, W. M. Heckl, T. G. Gopakumar and G. W. Flynn, "Molecular structures on crystalline metallic surfaces - From STM images to molecular electronics," *Microelectronic Engineering,* vol. 82, pp. 207-214, 2005.

[34] K. Mortensen, D. M. Chen, P. J. Bedrossian, J. A. Goloychenko and F. Besenbacher, "Two reaction channels directly observed for atomic hydrogen on the Si(111)-7x7 surface," *Physical Review,* vol. B 43, no. 2, p. 1816, 1991.

[35] J. J. Boland, "Nature of the Hydride Species on the Hydrogenated Si(111)-(7x7) Surface," *Journal of Physical Chemistry,* vol. 95, pp. 1521-1524, 1991.

[36] J. J. Boland, "Scanning tunneling microscopy of the interaction of hydrogen with silicon surfaces," *Advances in Physics,* vol. 42, no. 2, pp. 129-171, 1993.

[37] J. J. Boland, "The importance of structure and bonding in semiconductor surface chemistry: hydrogen on the Si(111)-7x7 surface," *Surface Science,* vol. 244, pp. 1-14, 1991.

[38] M. Fehrenbacher, J. Spitzmüller, U. Memmert, H. Rauscher and R. J. Behm, "Interaction of SiH_4 with Si(100)2x1 and with Si(111)7x7 at 690 K: A comparative scanning tunneling microscopy," *Journal of Vacuum Science & Technology A,* vol. 14, p. 1499, 1996.

[39] M. Nishijima, K. Edamoto, Y. Kubota, S. Tanaka and M. Onchi, "Vibrational electron energy loss spectroscopy of the Si(111)(7x7)-$H_2O(D_2O)$ system," *Journal of Chemical Physics,* vol. 84, p. 6458, 1986.

[40] S. Kitamura, T. Sato and M. Iwatsuki, "Observation of surface reconstruction on silicon above 800 °C using STM," *Nature,* vol. 351, pp. 215-217, 1991.

[41] A. Kirakosian, J. -L. Lin, D. Y. Petrocykh, J. N. Crain and F. J. Himpsel, "Functionalization of silicon step arrays I: Au passivation of stepped Si(111) templates," *Journal of Applied Physics,* vol. 90, no. 7, pp. 3286-3290, 2001.

[42] M. Miyazaki and H. Hirayama, "Thickness- and deposition temperature-dependent morphological change in electronic growth of ultra-thin Ag films on Si(111) substrates," *Surface Science,* vol. 602, pp. 276-282, 2008.

[43] M. Yoshimura, S. Shinabe and T. Yao, "Growth and annihilation of nickel silicide studied by scanning tunneling microscopy," *Surface Science,* Vols. 357-358, pp. 917-920, 1996.

[44] T. Ichikawa, T. Onodera and A. Mizoguchi, "High-Temperature Scanning Tunneling Microscopy Study of Si(111) Surface Structure Changes Caused by Ga Surface Diffusion," *Japanese Journal of Applied Physics,* vol. 41, pp. 2176-2182, 2002.

[45] M.-L. Tao, Y.-B. Tu, K. Sun, Y.-L. Wang, Z.-B. Xie, L. Liu, M.-X. Shi and J.-Z. Wang, "Gallenene epitaxially grown on Si(111)," *2D Materials,* vol. 5, no. 035009, 2018.

[46] J. Kraft, S. L. Surnev and F. P. Netzer, "The structure of the indium-Si(111)(√7x√3) monolayer surface," *Surface Science,* vol. 340, pp. 36-48, 1995.

[47] R. E. Honig, "Vapore Pressure Data for the Solid and Liquid Elements," *RCA Review,* vol. 23, p. 567, 1962.

[48] S. M. Sze, Physics of Semiconductor Devices, 2nd Edition, New York: John Wiley & Sons, 1981.

[49] Y. Shapira and D. Lichtman, "Properties of materials used in vacuum technology," in *Vacuum Physics and Technology*, New York, Academic Press, 1979, p. 345.

[50] A. A. van Gorkum, K. Nakagawa and Y. Shiraki, "Growth and characterization of atomic layer doping structures in Si," *Journal of Applied Physics,* vol. 65, p. 2485, 1989.

[51] N. Kishi and K. Morita, "Structure analysis of the Si(111)-3x3-Sb surface by means of CAICISS combined with LEED-AES-RBS techniques," *Current Applied Physics,* vol. 3, pp. 57-60, 2003.

[52] K. Nakagawa, S. Yamaguchi, N. Sugii and Y. Shiraki, "Reverse temperature dependence of Sb sticking on Si(100) surfaces," *Materials Science and Engineering,* vol. B 89, pp. 238-240, 2002.

[53] V. K. Paliwal, A. Vedeshwar and S. M. Shrivaprasad, "Sb induced (7x7) to (1x1) surface phase transformation of the Si(111) surface," *Solid State Communications,* vol. 127, pp. 7-11, 2003.

[54] C.-Y. Park, T. Abukawa, T. Kinoshita, Y. Enta and S. Kono, "Low Energy Electron Diffraction and X-Ray Photoelectrons Spectroscopy Studies of the Formation of Subomnolayer Interfaces of Sb/Si(111)," *Japanese Journal of Applied Physics,* vol. 27, no. 1, pp. 147-148, 1988.

[55] K. Yagi, H. Minoda and M. Degawa, "Step bunching, step wandering, and faceting: self-organization at Si surfaces," *Surface Science Reports,* vol. 43, pp. 45-126, 2001.

[56] K. Takayanagi, Y. Tanishiro, S. Takahashi and M. Takahashi, "Structure analysis of Si(111)-7x7 reconstructed surface by transmission electron diffraction," *Surface Science,* vol. 164, no. 2-3, pp. 367-392, 1985.

[57] Y. -N. Yang, E. S. Fu and E. D. Williams, "An STM study of current-induced step bunching on Si(111)," *Surface Science,* vol. 356, pp. 101-111, 1996.

[58] Y. Suzuki, M. Hietschold and D. R. Zahn, "Growth of Copper Phthalocyanine on hydrogen passivated vicinal silicon(111) surfaces," *Applied Surface Science,* vol. 252, no. 15, 2006. https://doi.org/10.1016/j.apsusc.2005.12.109

[59] Z. Bao, A. J. Loyinger and A. Dodabalapur, "Organic field-effect transistors with high mobility based on copper phthalocyanine," *Applied Physics Letter,* vol. 69, p. 3066, 1996.

[60] J. F. Yuan, J. Zhang, J. Wang, X. J. Yan, D. H. Yan and W. Xu, "Bottom-contact organic field-effect transistors having low-dielectric layer under source and drain electrodes," *Applied Physics Letters,* vol. 82, p. 3967, 2003.

[61] L. S. Hung and C. W. Tang, "Interface engineering in preparation of organic surface-emitting diodes," *Applied Physics Letters,* vol. 74, p. 3209, 1999.

[62] S. D. Wang, X. Dong, C. S. Lee and S. T. Lee, "Orderly Growth of Copper Phthalocyanine on Highly Oriented Pyrolytic Graphite (HOPG) at High Substrate Temperatures," *Journal of Physical Chemistry B,* vol. 108, no. 5, pp. 1529-1532, 2004.

[63] O. Gordan, M. Friedrich and D. R. Zahn, "Determination of the anisotropic dielectric function for metal free phthalocyanine thin films," *Thin Solid Films,* Vols. 455-456, pp. 552-556, 2004.

[64] O. Gordan, M. Friedrich and D. R. Zahn, "The anisotropic dielectric function for copper phthalocyanine thin films," *Organic Electronics,* vol. 5, no. 6, pp. 291-297, 2004.

[65] F. Rochet, G. Dufour, H. Roulet, N. Motta, A. Sgarlata, M. N. Piancastelli and M. De Crescenzi, "Copper phthalocyanine on Si(111)-7x7 and Si(100)-2x1: an XPS/AES and STM study," *Surface Science,* vol. 319, pp. 10-20, 1994.

[66] M. Roy and Y. Borensztein, "Hydrogen adsorption on Si surfaces studied by real-time surface reflectance spectroscopy," *Surface Science,* Vols. 331-333, pp. 453-457, 1995.

[67] K. Oura, V. G. Liftshits, A. A. Saranin, A. V. Zotov and M. Katayama, "Hydrogen interaction with clean and modified silicon surfaces," *Surface Science Reports,* vol. 35, pp. 1-69, 1999.

[68] R. L. Schwoebel and E. J. Shipsey, "Step Motion on Crystal Surfaces," *Journal of Applied Physics,* vol. 37, no. 10, p. 3682, 1966. https://doi.org/10.1063/1.1707904

[69] C. Teichert, G. Hlawacek, A. Winkler, P. Puschnig and C. Draxl, "Ehrlich-Schwoebel Barriers and Island Nucleation in Organic Thin-Film Growth," in *Small Organic Molecules on Surfaces. Springer Series in Materials Science,*, Springer, Berlin, Heidelberg, 2013, pp. 79-106.

[70] Y. Suzuki, T. Yamada, M. Hietschold and K. Okano, "Growth of Cu phthalocyanine thin films on Sb passivated vicinal Si(111) with molecular columns parallel to the surface," *Japanese Journal of Applied Physics,* vol. 59, p. 095001, 2020. https://doi.org/10.35848/1347-4065/aba9a4

[71] B. Voigtländer and M. Kästner, "Measurement of Sb diffusion using shadow profiles created by a STM tip," *Surface Science,* vol. 464, pp. 131-144, 2000.

[72] A. A. Saranin, A. V. Zotov, V. G. Lifshits, O. Kubo, T. Harada, M. Katayama and K. Oura, "Si(111)5√3×5√3-Sb: a surface phase with a variable composition," *Surface Science,* vol. 447, pp. 15-24, 2000.

[73] K. -H. Park, J. S. Ha, W. S. Yun and E. -H. Lee, "Initial stage of Ag epitaxial growth on Sb-terminated Si(111) surface," *Surface Science,* vol. 405, pp. 46-53, 1998.

[74] K.-H. Park, J. S. Ha, W. S. Yun, E.-H. Lee, J.-Y. Yi and S.-J. Park, "Scanning tunneling microscope study of Sb/Si(111)-5√3x5√3 structure," *Journal of Vacuum Science & Technology A,* vol. 15, p. 1572, 1997.

[75] T. M. Bernhardt, B. Stegemann, B. Kaiser and K. Rademann, "Crystalline Structures of Sb4 Molecules in Antimony Thin Films," *Angewandt Chemie,* vol. 42, no. 2, pp. 199-202, 2003.

[76] P. Kury, P. Zahl and M. Horn-von Hoegen, "Direct observation of reconstruction induced changes of surface stress for Sb on Si(111)," *Analytical Bioanalytical Chemistry,* vol. 379, no. 4, pp. 582-587, 2004.

[77] S. R. Wagner and P. Zhang, "Nucleation and evolution of zinc phthalocyanine thin films on the deactivated Si(111)-B√3 x √3 R30° surface," *Surface Science,* Vols. 22-27, no. 630, 2014.

[78] R. Hiesgen, M. Raebisch, H. Boettcher and D. Meissner, "STM investigation of the growth structure of Cu-phthalocyanine films with submolecular resolution," *Solar Energy Materials & Solar Cells,* vol. 61, pp. 73-85, 2000.

[79] G. Ehrlich and F. G. Hudda, "Atomic View of Surface Self-Diffusion: Tungsten on Tungsten," *Journal of Chemical Physics,* vol. 44, no. 3, p. 1039, 1966.

[80] P. Zimmermann, K. Majer, P. Kocan, I. Ostadal and P. Sobotik, "Role of Dangling Bond State Occupancy in Adsorpotion of Copper Phthalocyanine on Si(111)-Sn-√3x√3," *J. Phys. Chem.,* vol. 123, pp. 16232-16238, 2019.

[81] Y. Cao, K. S. Yong, Z. H. Wang, J. F. Deng, Y. H. Lai and G. Q. Xu, "Cycloaddition chemistry of thiophene on the silicon (111)-7x7 surface," *Journal of Chemical Physics,* vol. 115, no. 7, pp. 3287-3296, 2001. https://doi.org/10.1063/1.1386435

[82] K. Kaji, S.-L. Yau and K. Itaya, "Atomic scale etching processes of n-Si(111) in NH_4F solutions: in situ scanning tunneling microscopy," *Journal of Applied Physics,* vol. 78, no. 9, pp. 5727-5733, 1995. https://doi.org/10.1063/1.359633